

Massively Parallelized Interpolated Factored Green Function Method

Christoph Bauinger* and Oscar P. Bruno*

Abstract

This paper presents a parallel implementation of the “Interpolated Factored Green Function” (IFGF) method introduced recently for the accelerated evaluation of discrete integral operators arising in wave scattering and other areas (Bauinger and Bruno, *Jour. Computat. Phys.*, 2021). On the basis of the hierarchical IFGF interpolation strategy, the proposed (hybrid MPI-OpenMP) parallel implementation results in highly efficient data communication, and it exhibits in practice excellent parallel scaling up to large numbers of cores—without any hard limitations on the number of cores concurrently employed in an efficient manner. Moreover, on any given number of cores, the proposed parallel approach preserves the $\mathcal{O}(N \log N)$ computing cost inherent in the sequential version of the IFGF algorithm. Unlike other approaches, the IFGF method does not utilize the Fast Fourier Transform (FFT), and it is thus better suited than other methods for efficient parallelization in distributed-memory computer systems. A variety of numerical results presented in this paper illustrate the character of the proposed parallel algorithm, including excellent weak and strong parallel scaling properties in all cases considered—for problems of up to 4,096 wavelengths in electrical size, and scaling tests spanning from 1 compute core to all 1,680 cores available in the HPC cluster used.

Keywords: Parallelization, Green Function, Integral Equations, Acceleration, OpenMP, MPI, Distributed Memory Systems, High Performance Computing

1 Introduction

This paper presents a parallel implementation of the “Interpolated Factored Green Function” (IFGF) method introduced recently for the accelerated evaluation of discrete integral operators arising in wave scattering and other areas [1]. The proposed implementation, which is structured as a hybrid MPI-OpenMP computer program suitable for instantiation in modern high-performance computing systems (HPC), demonstrates in practice excellent parallel scaling up to large numbers of cores, without any hard limitations on the number of cores concurrently employed in an efficient manner, while preserving the linearithmic complexity (namely, $\mathcal{O}(N \log N)$ computing cost) inherent in the sequential IFGF algorithm. The IFGF method accelerates the evaluation of discrete integral operators by relying on a certain factorization of the Green function into two factors, a

*Computing and Mathematical Sciences, Caltech, Pasadena, CA 91125, USA

“centered factor” that is incorporated easily as a common factor in the calculation, and an “analytic factor” which enjoys a property of analyticity up to and including infinity—and which thus motivates the IFGF strategy, namely, evaluation of a given discrete integral operator by means of a hierarchical interpolation approach which relies on use of a large number of small and independent interpolation procedures. In particular, the IFGF approach does not utilize acceleration elements commonly used by other acceleration methods [2–13] such as the Fast Fourier Transform (FFT), special-function expansions, high-dimensional linear-algebra factorizations, translation operators, equivalent sources, or parabolic scaling. A variety of numerical results presented in this paper illustrate the character of the proposed parallel method, including excellent weak and strong parallel scaling properties in all cases considered—for problems of up to 4,096 wavelengths in electrical size, and scaling tests spanning from 1 compute core to all 1,680 cores available in the HPC cluster used.

The parallelization of accelerated Green function methods has been the subject of a significant literature, which is mostly devoted to tackling a particular difficulty, namely, the “parallelization bottleneck”—which manifests itself under various related guises [14–22], and which almost invariably concerns uses of the hard-to-parallelize [23] FFT algorithm. (Reference [24, Sec. 7], for example, mentions two alternatives to the use of FFTs in the context of the FMM, which, however, it discards as less efficient than an FFT-based procedure.) In the case of the multilevel Fast Multipole Method (FMM), the parallelization bottleneck arises in the evaluation of translation operators associated with the upper part of the octree structure, which leads to low parallel efficiency [2, 14, 19]. In the “directional” FMM [14] the low efficiency in the upper octree is alleviated as a result of the parabolic scaling utilized; however, the parallelization strategy does suffer from hard limitations in the number of parallel tasks that, in the cases considered in that reference, lead to a “leveling off” of the parallel scaling at 256 or 512 cores [14, Secs. 3.6, 4.2], depending on the geometry under consideration. Reference [15] identifies the part of the FMM relying on FFTs as a parallelization bottleneck which arises from FFT-related “lowest arithmetic intensity” and “bandwidth contention”. In [16, 17], in turn, a hybrid octree storage strategy is used, which stores a complete set of tree nodes for a certain number of “full” levels in each process, and which reduces the communication in the upper octree levels: this article demonstrates treatment of problems containing very large numbers of discretization points on up to 2,560 processes, but it restricts its description of the algorithm’s parallel efficiency to a limited strong scaling test from 1 process (sequential) to 64 processes. In contrast to this hybrid octree-storage strategy, reference [18] simultaneously partitions boxes (clusters) and field values representing the radiating and incoming fields of each box. This approach leads to increased efficiency compared to a parallelization purely based on the boxes (clusters), but the communication in the translation step still poses a bottleneck, resulting in as little as 30% parallel efficiency from one (sequential) core to 128 cores. To avoid the communication bottleneck in the upper multilevel FMM octree, references [19, 20] utilize a single-level Fast Multipole strategy. While this method significantly simplifies the algorithm and minimizes the required communication in a parallel setting, it does give rise to a sub-optimal asymptotic computational cost (e.g. $\mathcal{O}(N^{3/2})$ in [20] or, exploiting the FFT, $\mathcal{O}(N^{4/3} \log^{2/3} N)$ in [19]), and, while resulting in good parallel scaling up to 512 processes in the $\mathcal{O}(N^{3/2})$ algorithm [20], as in the case of [14], the parallel efficiency does level off beyond 512 processes.

Direct FFT methods present alternatives to the various FMM strategies, including, for example, the Adaptive Integral Method [10] (AIM) and the sparse-FFT method [9]. Like the single-level FMM algorithms, these FFT methods exhibit sub-optimal algorithmic complexity (of orders $\mathcal{O}(N^{3/2})$ and $\mathcal{O}(N^{4/3})$, respectively, and, owing to their strong reliance on FFTs, they also tend to suffer from reduced parallel efficiency, as shown and discussed for the AIM in e.g. [21, 22]. (A parallel version of

the algorithm [9], which has been developed by the authors, has not been published, but we report here that, as may have been expected, the overall parallel efficiency of the method suffers from the typical FFT-related degradation.) Finally, we mention the parallel Butterfly Method [25] which, although not applicable to singular Green function kernels such as the ones considered here, it does provide an acceleration technique for Fourier integral operators. Based on linear-algebra constructs instead of the hierarchical interpolation underlying the IFGF approach, the butterfly incorporates a parallelization strategy that is somewhat reminiscent of the proposed IFGF parallelization approach. The Blue Gene/Q implementation [25] of the Butterfly parallel algorithm demonstrates excellent results in terms of parallel scaling to a large number of cores.

The parallel IFGF strategy introduced in this contribution is based on adequately partitioning the interpolations performed on each level of the underlying octree structure, which facilitates the spatial decomposition of the surface discretization points. As shown in [1], the number of interpolations performed on each level is large and approximately constant (as a function of the octree level). The decomposition and distribution of the interpolation data is based on a total order in the set of spherical cone segments representing the interpolation domains. In view of its strong reliance on the box-cone structure inherent in the IFGF method, the proposed parallelization strategy is not applicable to other acceleration methods such as the FMM. The present parallel IFGF implementation on a 30-node (1,680-core) HPC cluster with Infiniband interconnect, delivers perfect $\mathcal{O}(N \log N)$ performance on all 1,680 cores, and, with high (albeit imperfect) strong and weak parallel efficiencies, unlike other methods, it does not suffer from scaling limitations, under either weak scaling and strong scaling tests, as the number of processing cores grow—conceivably, as argued in Sections 3.2 and 4, up to arbitrarily large numbers of cores.

This paper is organized as follows. Section 2 briefly summarizes the description [1] of the IFGF method, and it introduces the required notations and nomenclature. Section 3 then introduces the proposed parallelization strategy, including a description of the associated OpenMP and MPI parallelization approaches in Sections 3.1 and 3.2, respectively, and, then, in Section 3.3, a discussion its linearithmic communication costs—which results in preservation of the overall IFGF linearithmic parallel computing cost. A variety of numerical results are presented in Section 4 and, with additional detail, in the supplementary materials Section SM1. A few concluding comments, finally, are presented in Section 5.

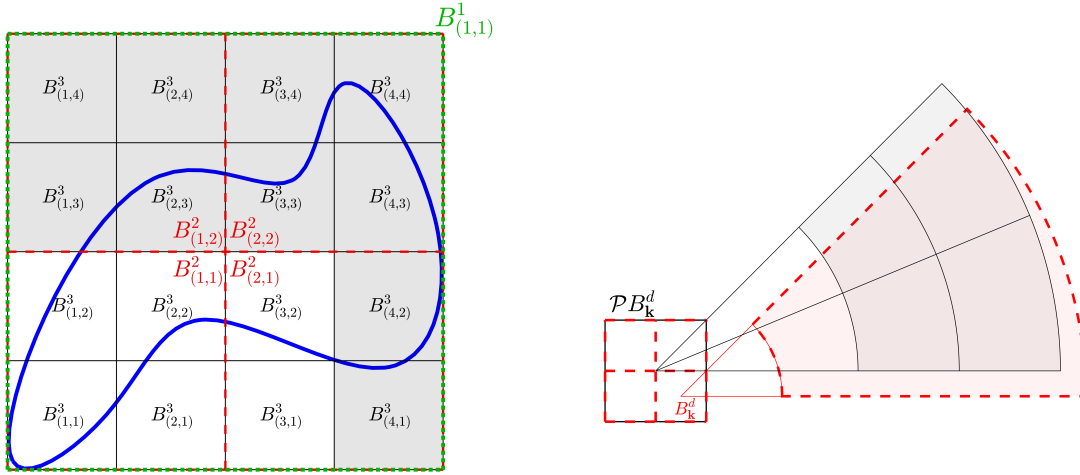
2 Review of the IFGF Method

As discussed above, the IFGF method provides an accelerated algorithm, requiring $\mathcal{O}(N \log N)$ operations, for the numerical evaluation of discrete integral operators of the form

$$I(x_\ell) := \sum_{\substack{m=1 \\ m \neq \ell}}^N a_m G(x_\ell, x_m), \quad \ell = 1, \dots, N, \quad (1)$$

for given points x_ℓ on a surface $\Gamma \subset \mathbb{R}^3$, and for given complex coefficients $a_m \in \mathbb{C}$, where the function $G(x, y)$, defined for $x, y \in \mathbb{R}^3$, denotes a Green function for some partial differential equation, such as the acoustic Green function

$$G(x, y) = \frac{e^{i\kappa|x-y|}}{4\pi|x-y|}$$



(a) Two-dimensional sketch of a three level ($D = 3$) IFGF domain decomposition with neighbors (in white) and cousin boxes (in gray) for the particular box $B_{(2,1)}^3$. A surrogate scatterer is sketched in blue.

(b) Two-dimensional illustration of cone segments: in red, cone-segments co-centered with the box $B_{\mathbf{k}}^d$, and, in black, cone-segments co-centered with the parent box $\mathcal{P}B_{\mathbf{k}}^d$.

Figure 1: Illustration of the box and cone hierarchical structures used in the IFGF method.

associated with the Helmholtz equation (ι denotes the imaginary unit and κ the wavenumber) as well as those associated with the Laplace, Stokes, and elasticity equations, among others. In what follows we denote by $\Gamma_N := \{x_1, \dots, x_N\} \subset \Gamma$ the set of surface discretization points.

For a given $D \in \mathbb{N}$, the IFGF method is based upon use of a D -level octree hierarchical decomposition of a cube $B_{1,1,1}^1$ containing the discrete surface Γ_N , where each level is determined by a set of axis-aligned boxes $B_{\mathbf{k}}^d \subset \mathbb{R}^3$ (defined as the Cartesian product of three one-dimensional half-open intervals of the form $[a, a + H_d)$ for some $a \in \mathbb{R}$), where $\mathbf{k} \in \mathbb{N}^3$ denotes a multi-index describing the three-dimensional position of the box in the resulting Cartesian grid of boxes, and where d ($1 \leq d \leq D$) denotes the level in the octree. The octree structure of boxes is defined iteratively starting from a single box $B_{1,1,1}^1 \supset \Gamma_N$ of side $H_1 \in \mathbb{R}$, $H_1 > 0$, on level $d = 1$. (Note that there is no undue expense incurred for, say, an elongated surface Γ , for which a cubic box could be mostly empty—since, as indicated in what follows, only certain “relevant” child boxes in the box octree are used by the algorithm.) The boxes on consecutive levels $d = 2, \dots, D$ are defined by means of a partition of each of the level $(d - 1)$ boxes into eight equi-sized and disjoint boxes of side $H_d = H_{d-1}/2$ resulting in the level d boxes $B_{\mathbf{k}}^d$ ($\mathbf{k} \in \{1, \dots, 2^{d-1}\}^3 =: I_B^d$). The two-dimensional equivalent of the resulting hierarchical octree structure for an illustrative three-level configuration ($D = 3$) is depicted in Figure 1a. Clearly, each box $B_{\mathbf{k}}^d$ on level d ($2 \leq d \leq D$) admits a unique $(d - 1)$ -level parent box $\mathcal{P}B_{\mathbf{k}}^d$ containing $B_{\mathbf{k}}^d$.

To achieve the desired acceleration, the IFGF method only considers interactions between boxes in a certain set \mathcal{R}_B of *relevant boxes*, which are defined as the boxes in the octree structure that contain at least one surface discretization point:

$$\mathcal{R}_B^d := \{B_{\mathbf{k}}^d : \Gamma_N \cap B_{\mathbf{k}}^d \neq \emptyset, \mathbf{k} \in I_B^d\}, \quad d = 1, \dots, D,$$

$$\mathcal{R}_B := \bigcup_{d=1, \dots, D} \mathcal{R}_B^d.$$

Furthermore, for a given box $B_{\mathbf{k}}^d$ on any level d , the method relies on a number of additional concepts, such as the *set of neighboring boxes* $\mathcal{N}B_{\mathbf{k}}^d$ (namely the set of level- d boxes whose closure have a non-empty intersection with the closure $\overline{B_{\mathbf{k}}^d}$ of $B_{\mathbf{k}}^d$) and the *set of cousin boxes* $\mathcal{M}B_{\mathbf{k}}^d$ (non-neighboring boxes that are children of the parents neighbors), as well as related concepts such as the *set of neighboring points* $\mathcal{U}B_{\mathbf{k}}^d$ and the *set of cousin points* $\mathcal{V}B_{\mathbf{k}}^d$ (which denote the set of surface discretization points within the neighboring boxes and the cousin boxes, respectively):

$$\begin{aligned}\mathcal{N}B_{\mathbf{k}}^d &:= \{B_{\mathbf{j}}^d \in \mathcal{R}_B : \|\mathbf{j} - \mathbf{k}\|_{\infty} \leq 1\}, \\ \mathcal{M}B_{\mathbf{k}}^d &:= \{B_{\mathbf{j}}^d \in \mathcal{R}_B : B_{\mathbf{j}}^d \notin \mathcal{N}B_{\mathbf{k}}^d \wedge \mathcal{P}B_{\mathbf{j}}^d \in \mathcal{N}\mathcal{P}B_{\mathbf{k}}^d\}, \\ \mathcal{U}B_{\mathbf{k}}^d &:= \left(\bigcup_{B \in \mathcal{N}B_{\mathbf{k}}^d} B \right) \cap \Gamma_N, \\ \mathcal{V}B_{\mathbf{k}}^d &:= \left(\bigcup_{B \in \mathcal{M}B_{\mathbf{k}}^d} B \right) \cap \Gamma_N.\end{aligned}\tag{2}$$

Figure 1a displays the neighbors and cousins of the box $B_{(2,1)}^3$ in white and gray colors, respectively.

The IFGF algorithm accelerates the evaluation of the operator (1) by exploiting a fast method for evaluation of pairwise interactions between cousin boxes on every level d , for $d = D, \dots, 3$. (Note that the algorithm ends at level $d = 3$ —since at $d = 3$, each box is a cousin or a neighbor of all the other boxes, and thus, all remaining surface evaluations are completed at this stage.) The evaluation of these interactions is enacted by means of a simple piecewise interpolation method based on a certain factored form of the Green function in a set of box-centered spherical coordinate systems, with one such spherical-coordinate system centered at each one of the relevant boxes. The use of angular and radial interpolation methods gives rise to so-called *cone segments* $C_{\mathbf{k};\gamma}^d$: one for each box $B_{\mathbf{k}}^d$ and for each multi-index $\gamma \in I_C^d \subset \mathbb{N}^3$ characterizing a conical interpolation domain. A set $\mathcal{X}C_{\mathbf{k};\gamma}^d$ of $P \in \mathbb{N}$ *interpolation points* is used within each cone segment $C_{\mathbf{k};\gamma}^d$, where P is an arbitrary but fixed number throughout the algorithm. In what follows, cone segments $C_{\mathbf{k};\gamma}^d$ are called *co-centered* with a box $B_{\mathbf{k}}^d$ if and only if the origin of the spherical coordinate system defining the cone segment coincides with the center of the box. Two cone segments are called *co-centered* if they are co-centered with the same box. Note that the sub- and super indices \mathbf{k} and d in the cone-segment notation $C_{\mathbf{k};\gamma}^d$ coincide with the corresponding indices of the co-centered box.

To achieve competitive computation times, a certain factorization of the Green function $G(x, x') = G(x, x_{\mathbf{k}}^d)g_{\mathbf{k}}^d(x, x')$ into a *centered* factor $G(x, x_{\mathbf{k}}^d)$ (centered at the *box-center* $x_{\mathbf{k}}^d$ of the box $B_{\mathbf{k}}^d$) and an *analytic* factor $g_{\mathbf{k}}^d(x, x')$, is used. The field $I(x)$ in (1) can be expressed for each level d as the sum over all multi-indices $\mathbf{k} \in I_B^d$ of fields $I_{\mathbf{k}}^d(x)$ generated by point sources placed at the surface discretization points $x' \in B_{\mathbf{k}}^d \cap \Gamma_N$ within the box $B_{\mathbf{k}}^d$. (The field, as a function of $x \in \mathbb{R}^3$, generated by such a point source is expressed through the Green function $G(x, x')$, where one coordinate is fixed to the position x' of the point source.) Using the aforementioned factorization centered at $x_{\mathbf{k}}^d$ yields

$$I_{\mathbf{k}}^d(x) = \sum_{x' \in B_{\mathbf{k}}^d \cap \Gamma_N} a(x')G(x, x') = G(x, x_{\mathbf{k}}^d)F_{\mathbf{k}}^d(x), \quad F_{\mathbf{k}}^d(x) := \sum_{x' \in B_{\mathbf{k}}^d \cap \Gamma_N} a(x')g_{\mathbf{k}}^d(x, x'), \tag{3}$$

where $a(x')$ denotes the coefficient a_m in (1) that corresponds to the point $x' \in \Gamma_N$. The IFGF interpolation procedure is then used to evaluate $F_{\mathbf{k}}^d$. The generation of the P coefficients of each

one of the degree- P polynomial interpolants $I_P C_{\mathbf{k};\gamma}^d$, corresponding to interpolation of the field $F_{\mathbf{k}}^d$ (cf. 3) over the cone segment $C_{\mathbf{k};\gamma}^d$, is achieved on the basis of the field values $F_{\mathbf{k}}^d(\mathcal{X}C_{\mathbf{k};\gamma}^d) := \{F_{\mathbf{k}}^d(x) : x \in \mathcal{X}C_{\mathbf{k};\gamma}^d\}$.

In [1] it is shown that the analytic factor is analytic everywhere in $\mathbb{R}^3 \setminus \mathcal{N}B_{\mathbf{k}}^d$ and up to and including infinity, and it can therefore be interpolated accurately throughout that region on the basis of a small (finite!) number of interpolation points. (It is easy to check that the same is true for most of the relevant kernels arising in applications.) Since $F_{\mathbf{k}}^d$ equals a linear combination of finitely many analytic-factor functions, it is clear that this function shares the same analytic properties, and it can therefore be interpolated with equal quality and efficiency.

The cone segments $C_{\mathbf{k};\gamma}^d$ are defined by means of an iterative procedure similar to the one used in the definition of the boxes $B_{\mathbf{k}}^d$, but in reversed order starting from $d = D$ and moving upwards the tree to $d = 3$. The set of cone segments that is to be used at a given level d depends strongly on the character of the surface Γ_N , the wavenumber κ and, possibly, the Green function G . A two-dimensional sketch of some illustrative box-centered cone segments for a given box $B_{\mathbf{k}}^d$ and its parent $\mathcal{P}B_{\mathbf{k}}^d$ is provided in Figure 1b.

To achieve the claimed acceleration and perform the computation of (1) in $\mathcal{O}(N \log N)$ operations, the IFGF algorithm uses iterated interpolation to evaluate the analytic factor at the interpolation points of consecutive levels, avoiding the cost of re-evaluating the field $I_{\mathbf{k}}^d(x)$ on every level through the use of the interpolation data on level d to generate the interpolants on level $(d-1)$ for $d = D, \dots, 4$. In order to further increase the efficiency and achieve the desired $\mathcal{O}(N \log N)$ complexity, as is done for boxes, the IFGF method only utilizes the set of *relevant cone segments* $\mathcal{R}_C B_{\mathbf{k}}^d$ for each box $B_{\mathbf{k}}^d$, namely, the cone segments that are used for interpolation back to cousin surface discretization points or to relevant cone segments on the parent level,

$$\begin{aligned} \mathcal{R}_C B_{\mathbf{k}}^d &:= \emptyset \quad \text{for } d = 1, 2, \\ \mathcal{R}_C B_{\mathbf{k}}^d &:= \left\{ C_{\mathbf{k};\gamma}^d : \gamma \in I_C^d, C_{\mathbf{k};\gamma}^d \cap \mathcal{V}B_{\mathbf{k}}^d \neq \emptyset \text{ or } C_{\mathbf{k};\gamma}^d \cap \left(\bigcup_{C \in \mathcal{R}_C \mathcal{P}B_{\mathbf{k}}^d} C \right) \neq \emptyset \right\} \quad \text{for } d \geq 3. \end{aligned} \quad (4)$$

The serial IFGF algorithm, introduced in [1], is summarized in Algorithm 1. Note that the algorithm does not address the interactions between neighboring boxes on the lowest level D . The latter contributions are to be produced by means of a separate algorithm, namely, direct summation in the present context of the discrete operator (1), or some local integration algorithm for surface scattering problems, etc.

3 Parallel IFGF Method

Our IFGF parallelization approach is designed for implementation in modern high-performance computing (HPC) *cluster* systems. The architecture of such systems is briefly described in what follows; more detailed descriptions and alternative hardware designs can be found e.g. in [26, 27]. A modern computer cluster consists of multiple compute *nodes*. Each node contains its own memory space, and thus the memory in the cluster is distributed between the nodes. In particular, access to memory in other compute nodes requires explicit data communication, which is typically performed via the *message passing interface* (MPI) [27, Section 8]; the performance of algorithmic implementations for cluster systems can significantly benefit from careful engineering of MPI-based inter-process data communications.

Algorithm 1 IFGF Method

```
1: \\Direct evaluations on the lowest level.
2: for  $B_{\mathbf{k}}^D \in \mathcal{R}_B$  do
3:   for  $C_{\mathbf{k};\gamma}^D \in \mathcal{R}_C B_{\mathbf{k}}^D$  do                                ▷ Evaluate  $F$  at all relevant interpolation points
4:     Evaluate and store  $F_{\mathbf{k}}^D(\mathcal{X}C_{\mathbf{k};\gamma}^D)$ 
5:     Generate interpolant  $IPC_{\mathbf{k};\gamma}^D$ 
6:   end for
7: end for
8:
9: \\Interpolation onto surface discretization points and parent interpolation points.
10: for  $d = D, \dots, 3$  do
11:   for  $B_{\mathbf{k}}^d \in \mathcal{R}_B$  do
12:     for  $x \in \mathcal{V}B_{\mathbf{k}}^d$  do                                          ▷ Interpolate at cousin surface points
13:       Determine  $C_{\mathbf{k};\alpha}^d$  s.t.  $x \in C_{\mathbf{k};\alpha}^d$ 
14:       Evaluate and add to result  $IPC_{\mathbf{k};\alpha}^d(x) \times G(x, x_{\mathbf{k}}^d)$ 
15:     end for
16:     if  $d > 3$  then                                                ▷ Evaluate  $F$  on parent interpolation points
17:       Determine parent  $B_{\mathbf{j}}^{d-1} = \mathcal{P}B_{\mathbf{k}}^d$ 
18:       for  $C_{\mathbf{j};\gamma}^{d-1} \in \mathcal{R}_C B_{\mathbf{j}}^{d-1}$  do
19:         for  $x \in \mathcal{X}C_{\mathbf{j};\gamma}^{d-1}$  do
20:           Determine  $C_{\mathbf{k};\alpha}^d$  s.t.  $x \in C_{\mathbf{k};\alpha}^d$ 
21:           Evaluate and add  $IPC_{\mathbf{k};\alpha}^d(x) \times G(x, x_{\mathbf{k}}^d)/G(x, x_{\mathbf{j}}^{d-1})$ 
22:         end for
23:       end for
24:     end if
25:   end for                                                         ▷ Generate interpolants on parent level
26:   for  $B_{\mathbf{j}}^{d-1} \in \mathcal{R}_B$  do
27:     for  $C_{\mathbf{j};\gamma}^{d-1} \in \mathcal{R}_C B_{\mathbf{j}}^{d-1}$  do
28:       Generate interpolant  $IPC_{\mathbf{j};\gamma}^{d-1}$ 
29:     end for
30:   end for
31: end for
```

Each node typically comprises one or a few *multi-core processors*, each one of which, as the name suggests, contains multiple computing *cores*. The compute nodes are so-called *shared memory machines* (SMMs), where each core within the node can access all of the memory in the node. To efficiently make use of more than a single core, certain specialized programming techniques are required, e.g. the Intel Threading Building Blocks (TBB) library, the C++ standard threading model, MPI, or the OpenMP programming interface. Modern compute nodes usually follow a non-uniform memory access (NUMA) design (in contrast to uniform memory access (UMA)), where the access times to the shared memory depend on the locality of the memory with respect to the multi-core processor accessing it. This design typically results in multiple NUMA nodes per compute node, where memory access to other NUMA nodes on the same compute node is usually significantly slower than access to memory local to the processor. All of the tests presented in this paper were conducted on a small cluster consisting of thirty nodes connected via an InfiniBand interconnect, each one of

which contains four fourteen-core NUMA nodes; additional details concerning the hardware used are provided in Section 4 and Supplementary Materials Sections SM1.1 and SM1.2.

On the basis of the functions and synchronization capabilities provided by MPI, a program can be launched as a set of multiple *processes* (which are identified in what follows by their corresponding integer-valued *rank* within the group of all processes launched by a given program). One of the main roles of the MPI standard is to allow the programmer to orchestrate the data communications between the ranks. Note that, at runtime, an MPI rank can be assigned, or *pinned*, to various kinds of hardware units, such as e.g. a single core, a NUMA node, a complete compute node, or various combinations of cores and/or nodes.

The IFGF parallelization scheme proposed in this paper relies on use of a hybrid MPI-OpenMP approach. As detailed in Section 3.2, the MPI interface plays two distinct roles in the proposed scheme: it is used to enable distributed-memory parallelization across compute nodes and to distribute work and handle memory access (while still relying on shared memory) across NUMA nodes within each compute node. This guarantees that memory held by a certain MPI rank is stored within a single NUMA node and can therefore be accessed quickly by all cores within the NUMA node. Accessing memory in a different NUMA node is facilitated through MPI as efficiently as possible, in the same manner as the memory transfers are facilitated between compute nodes through MPI. The OpenMP parallelization, as described in Section 3.1, is used to distribute the work to the hardware residing within each NUMA node by pinning each OpenMP thread to a single hardware core. Hence, in the specific hardware implementation demonstrated in this paper, four intra-node MPI ranks are used per compute node, each pinned to a single NUMA node, each one of which spawns fourteen OpenMP threads. Up to one-hundred and twenty MPI ranks are used across the thirty available compute nodes, finally, enabling parallelization of the program up to and possibly including the complete cluster.

Clearly, the proposed hybrid MPI-OpenMP parallelization strategy could be abandoned in favor of a pure MPI parallelization, where each MPI rank is pinned to a single core, discarding the OpenMP parallelization completely. Or, conversely, it would also be possible to use MPI purely for the distributed-memory parallelization, assigning each compute node only a single MPI rank, and using OpenMP for the shared-memory parallelization, effectively ignoring the NUMA nodes in the OpenMP parallelization strategy. Considering the increased difficulty arising from the implementation and maintenance of a hybrid code, which we advocate, either of the approaches described above, based on a single parallelization technique on each compute node, might be considered preferable. However, our tests have shown that, for our algorithm and on the hardware we use, the proposed hybrid MPI-OpenMP parallelization nearly halves the computing time relative to pinning each MPI thread to a complete compute node—without the adverse impact on code complexity (in case MPI-3 shared-memory windows are used to facilitate intra-node memory accesses), memory (due to data shared between MPI ranks), or communication overhead (in case intra-node communications are facilitated explicitly through MPI) that would result from use of pure MPI parallelism within each node. The favorable performance of the hybrid approach, may be attributed to 1) A highly optimized MPI communication scheme, which minimizes the number of memory exchanges between NUMA nodes by transferring and storing adequately selected data groups, and thereby avoids repeated OpenMP access across NUMA nodes, and 2) The fast memory access times within a single NUMA node. A discussion on the performance of hybrid MPI-OpenMP approaches can be found in [28–30].

The OpenMP and the MPI elements of the overall parallelization strategy are considered separately in Sections 3.1 and 3.2, respectively.

3.1 OpenMP parallelization

Before introducing the proposed OpenMP parallelization scheme, we briefly consider a straightforward OpenMP parallelization strategy which we do not recommend but which we present for reference. This straightforward and easily implemented strategy results by simply assigning the work associated with groups of relevant boxes to various OpenMP threads (e.g. with a “#pragma omp parallel for” statement), in such a way that each group is handled by a single thread. Equi-distribution of relevant boxes onto the OpenMP threads implies equi-distribution of both the surface discretization points and the computations performed per thread—but only provided 1) The surface discretization points are roughly equi-distributed among the relevant boxes, and, 2) There is a sufficient number of relevant boxes to occupy all OpenMP threads. The difficulties associated with point 1) could be negotiated, in view of the law of large numbers [31, Section 13], provided sufficiently many boxes are used, that is to say, provided point 2) is satisfied. In other words, the feasibility of the approach under consideration hinges on the existence of sufficiently many relevant boxes on each level, as required by point 2). Unfortunately, however, for any given discretized surface Γ_N , point 2) is not satisfied at certain levels d in the octree structure, unless only a small number of threads is employed. Noting that, for any surface Γ_N , there are only sixty-four boxes overall on level $d = 3$ of the algorithm (and, in general, even fewer relevant boxes), we see that a definite limit exists on the parallelism achievable by this approach. The method presented in [14] uses this strategy in an MPI context, and it is therefore subject to such a hard limitation on achievable parallelism (although in a somewhat mitigated form, owing to the characteristics of that algorithm, as discussed in Section 1). To avoid such limitations we consider an alternate OpenMP parallelization strategy specifically enabled by the characteristics of the IFGF algorithm, as described in what follows.

The proposed strategy proceeds via parallelization of the three independent programming functions that comprise the IFGF method, namely the *LevelDEvaluations* function, the *Interpolation* function and the *Propagation* function. The first of these functions, the *LevelDEvaluations* function, which corresponds to the loop in line 2 of Algorithm 1, evaluates, for each relevant level- D box, the field generated by the point sources within the box (given by (3) with $d = D$) at the interpolation points in all relevant cone segments co-centered with the box and generates the required interpolants. The second function, the level- d -dependent *Interpolation* function, which corresponds to line 14 under the loops in lines 12 and 13, performs the necessary interpolations to cousin surface discretization points on level d ($d = 3, \dots, D$). The third and final programming function, the level- d -dependent *Propagation* function, which corresponds to line 20 under the loops in lines 12, 18, and 19, interpolates, for each relevant level- d box, to interpolation points in the relevant cone segments co-centered with the parent box on level $(d - 1)$ and generates the required interpolants. These three functions are outlined in Algorithms 2, 3, and 4, respectively. Using these three functions, the IFGF algorithm (Algorithm 1) may be re-expressed as Algorithm 5. In what follows, we present our strategies for efficient parallelization of each one of these functions separately.

Our approach for an efficient parallelization of the *LevelDEvaluations* function is based on changing the viewpoint from iterating through the level- D relevant boxes to iterating through the set \mathcal{R}_C^D of *all relevant cone segments on level D* . Since corresponding sets of level- d relevant cone segments for the wider range $3 \leq d \leq D$ are utilized in the parallelization of the *Propagation* function, we generalize the definition: the set of *all relevant cone segments on level d* is denoted by \mathcal{R}_C^d , that is

$$\mathcal{R}_C^d := \bigcup_{\mathbf{k} \in I_B^d: B_{\mathbf{k}}^d \in \mathcal{R}_B} \mathcal{R}B_{\mathbf{k}}^d, \quad \text{for } 3 \leq d \leq D. \quad (5)$$

Algorithm 2 LevelDEvaluations

```
1: for  $B_{\mathbf{k}}^D \in \mathcal{R}_B$  do  
2:   for  $C_{\mathbf{k};\gamma}^D \in \mathcal{R}_C B_{\mathbf{k}}^D$  do  
3:     Evaluate and store  $F_{\mathbf{k}}^D(\mathcal{X}C_{\mathbf{k};\gamma}^D)$   
4:     Generate interpolant  $IPC_{\mathbf{k};\gamma}^D$   
5:   end for  
6: end for
```

Algorithm 3 Interpolation(d)

```
1: for  $B_{\mathbf{k}}^d \in \mathcal{R}_B$  do  
2:   for  $x \in \mathcal{V}B_{\mathbf{k}}^d$  do  
3:     Determine  $C_{\mathbf{k};\alpha}^d$  s.t.  $x \in C_{\mathbf{k};\alpha}^d$   
4:     Evaluate and add to result  $IPC_{\mathbf{k};\alpha}^d(x) \times G(x, x_{\mathbf{k}}^d)$   
5:   end for  
6: end for
```

Using (5), a parallel version of Algorithm 2 is presented in Algorithm 6. The aforementioned change in viewpoint corresponds to collapsing the two outermost nested loops in Algorithm 2, effectively increasing the number of independent tasks and, consequently, the achievable parallelism. Note that, in a C++ implementation, the “parallel for” construct in Algorithm 6 corresponds to e.g. a “for”-loop preceded by the pragma directive “omp parallel for”.

The proposed parallelization of the d -dependent *Propagation* function follows a similar idea as the parallel *LevelDEvaluations* considered above—relying now on iteration over the relevant ($d - 1$) (parent-level) cone segments, which are targets of the interpolation, instead of the relevant level- d boxes emitting the field. This strategy addresses the difficulties arising from the straightforward approach described at the beginning of Section 3.1, for which the number of available tasks to be distributed decreases with the level d and imposes a hard limit on the achievable parallelism. Indeed, in the context of the oscillatory Green functions over two-dimensional surfaces $\Gamma \subset \mathbb{R}^3$ considered in this paper, for example, wherein the number of relevant cone segments on each level is an approximately constant function of d [1, Sec. 3.3.3], the number of independent tasks available for parallelization remains approximately constant as a function of d . Additionally, the proposed parallel *Propagation* strategy avoids a significant “thread-safety” [32,33], predicament, that is ubiquitous in the straightforward approach, whereby multiple writes to the same target interpolation point on the parent level take place from different threads. In contrast, the proposed *Propagation* strategy, is by design thread-safe without any additional considerations, since it distributes the targets of the interpolation to the available threads. Note that the practical implementation of this approach requires the algorithm to first determine the relevant box

$$\mathcal{R}_B C_{\mathbf{k};\gamma}^d := B_{\mathbf{k}}^d \quad \text{s.t.} \quad C_{\mathbf{k};\gamma}^d \in \mathcal{R}_C B_{\mathbf{k}}^d \quad (6)$$

that is co-centered with a given relevant cone segment $C_{\mathbf{k};\gamma}^d$; then to determine the relevant level- $(d + 1)$ *child boxes*

$$\mathcal{C}B_{\mathbf{k}}^d := \{B_{\mathbf{j}}^{d+1} \in \mathcal{R}_B : \mathbf{j} \in I_B^{d+1}, \mathcal{P}B_{\mathbf{j}}^{d+1} = B_{\mathbf{k}}^d\}, \quad (7)$$

of a given relevant box $B_{\mathbf{k}}^d$ on level d ; and, finally, to find all the interpolants $IPC_{\mathbf{k};\gamma}^d$ on the relevant cone segments (4) co-centered with the child boxes from which the propagation needs to be enacted. Using this notation, the resulting *Parallel Propagation* algorithm is presented in Algorithm 7.

Algorithm 4 Propagation(d)

```
1: for  $B_{\mathbf{k}}^d \in \mathcal{R}_B$  do
2:   Determine parent  $B_{\mathbf{j}}^{d-1} = \mathcal{P}B_{\mathbf{k}}^d$ 
3:   for  $C_{\mathbf{j};\gamma}^{d-1} \in \mathcal{R}_C B_{\mathbf{j}}^{d-1}$  do
4:     for  $x \in \mathcal{X}C_{\mathbf{j};\gamma}^{d-1}$  do
5:       Determine  $C_{\mathbf{k};\alpha}^d$  s.t.  $x \in C_{\mathbf{k};\alpha}^d$ 
6:       Evaluate and add  $I_P C_{\mathbf{k};\alpha}^d(x) \times G(x, x_{\mathbf{k}}^d)/G(x, x_{\mathbf{j}}^{d-1})$ 
7:     end for
8:   end for
9: end for
10: for  $B_{\mathbf{j}}^{d-1} \in \mathcal{R}_B$  do
11:   for  $C_{\mathbf{j};\gamma}^{d-1} \in \mathcal{R}_C B_{\mathbf{j}}^{d-1}$  do
12:     Generate interpolant  $I_P C_{\mathbf{j};\gamma}^{d-1}$ 
13:   end for
14: end for
```

Algorithm 5 IFGF Method

```
1: LevelDEvaluations()
2:
3: for  $d = D, \dots, 3$  do
4:   Interpolation( $d$ )
5:   if  $d > 3$  then
6:     Propagation( $d$ )
7:   end if
8: end for
```

The proposed parallelization strategy for the third and final IFGF programming function, namely, the *Interpolation* function, relies once again on the strategy used for the *LevelDEvaluations* and *Propagation* functions—which, in the present case, leads to changing the viewpoint from iterating through the relevant boxes to iterating through the surface discretization points that are the target of the interpolation procedure. This approach avoids both, the difficulties mentioned at the beginning of Section 3.1 (concerning the existence of a small number of relevant boxes in the upper levels of the octree structure), as well as thread-safety difficulties similar to those discussed above in the context of the *Propagation* function. For a concise description of the parallel *Interpolation* function in what follows we denote by

$$\mathcal{M}^d(x) := \{B_{\mathbf{k}}^d \in \mathcal{R}_B : x \in \mathcal{V}B_{\mathbf{k}}^d\}, \quad (8)$$

the set of *cousin boxes* of a surface discretization point $x \in \Gamma_N$ on level d , $3 \leq d \leq D$, which extends

Algorithm 6 Parallel LevelDEvaluations

```
1: parallel for  $C_{\mathbf{k};\gamma}^D \in \mathcal{R}_C^D$  do
2:   Evaluate and store  $F_{\mathbf{k}}^D(\mathcal{X}C_{\mathbf{k};\gamma}^D)$ 
3:   Generate interpolant  $I_P C_{\mathbf{k};\gamma}^D$ 
4: end parallel for
```

Algorithm 7 Parallel Propagation(d)

```
1: parallel for  $C_{j;\gamma}^{d-1} \in \mathcal{R}_C^{d-1}$  do
2:   for  $B_{\mathbf{k}}^d \in \mathcal{C}(\mathcal{R}_B C_{j;\gamma}^{d-1})$  do
3:     for  $x \in \mathcal{X} C_{j;\gamma}^{d-1}$  do
4:       Determine  $C_{\mathbf{k};\alpha}^d$  s.t.  $x \in C_{\mathbf{k};\alpha}^d$ 
5:       Evaluate and add  $I_P C_{\mathbf{k};\alpha}^d(x) \times G(x, x_{\mathbf{k}}^d)/G(x, x_j^{d-1})$ 
6:     end for
7:   end for
8:   Generate interpolant  $I_P C_{j;\gamma}^{d-1}$ 
9: end parallel for
```

Algorithm 8 Parallel Interpolation(d)

```
1: parallel for  $x \in \Gamma_N$  do
2:   for  $B_{\mathbf{k}}^d \in \mathcal{M}^d(x)$  do
3:     Determine  $C_{\mathbf{k};\gamma}^d$  s.t.  $x \in C_{\mathbf{k};\gamma}^d$ 
4:     Evaluate  $I_P C_{\mathbf{k};\gamma}^d(x) \times G(x, x_{\mathbf{k}}^d)$ 
5:   end for
6: end parallel for
```

the concept of cousin boxes of a box, introduced in (2) in Section 2. Using the definition (8), the *Parallel Interpolation* function is stated in Algorithm 8.

In summary, the OpenMP parallelization strategies proposed above for the functions *Parallel LevelDEvaluations*, *Parallel Propagation* and *Parallel Interpolation* are thread-safe by design, and they provide effective work distribution by relying on iteration over items (relevant cone segments or surface discretization points) that exist in a sufficiently large (and essentially constant) quantities for all levels d , $3 \leq d \leq D$, in the box-octree structure. As a result, the proposed approach effectively eliminates the hard limitation present in the straightforward OpenMP parallelization scheme mentioned at the beginning of this section. Note that the proposed IFGF box-cone parallelization strategy is in general not applicable to other hierarchical acceleration methods, such as e.g. FMM-type algorithms. Indeed, in contrast to the incremental propagation and surface evaluation approach inherent in the IFGF method, previous acceleration methods rely on the FFT algorithm—which, as discussed in Section 1, leads to inefficiencies in the upper portions of the corresponding octree structures [2, 14].

3.2 MPI parallelization

The proposed MPI parallel IFGF algorithm, which enables both data distribution onto the MPI ranks and efficient communication of data between MPI ranks, mirrors the one proposed in Section 3.1 for the corresponding OpenMP interface. In fact, the MPI parallel scheme is based on slight modifications of the OpenMP parallel Algorithms 6, 7, and 8. As indicated by the theoretical discussion in Section 3.3, the communication overhead is such that the intrinsic IFGF linearithmic complexity previously demonstrated in [1] for a single core implementation is preserved on any fixed number N_c of cores; an illustration of this theoretical result on $N_c = 1,680$ cores is presented in the Supplementary Materials Table SM4. Most importantly, as in the OpenMP case (cf. the last paragraph of Section 3.1), for arbitrarily large numbers D of levels, the MPI IFGF algorithm iter-

ates over items (relevant cone segments or surface discretization points) that exist in a sufficiently large (and essentially constant) quantities for all levels d , $3 \leq d \leq D$, in the box-octree structure. As a result, the strategy results in an overall MPI-OpenMP IFGF parallel scheme without hard limitations on the achievable parallelism as the number of cores grows.

3.2.1 Problem decomposition and data distribution

The distribution of the data required by the IFGF algorithm to the MPI ranks can be summarized as the independent distribution of the set of surface discretization points Γ_N , which are organized on the basis of boxes induced by an octree structure, and the distribution of the set of relevant cone segments on each level \mathcal{R}_C^d . Clearly, for an efficient parallel implementation, the distribution used should balance the amount of work performed by each rank while maintaining a minimal memory footprint per rank and while also minimizing the communication between ranks. A concise description of the method used for data distribution to the MPI ranks is presented in what follows, where we let $N_r \in \mathbb{N}$ and $\rho \in \mathbb{N}$ ($1 \leq \rho \leq N_r$) denote the number of MPI ranks and the index of a specific MPI rank, respectively.

The distribution of the surface discretization points is orchestrated on the basis of an ordering of the set of relevant boxes \mathcal{R}_B^d on each level d , which, in the proposed algorithm, is obtained from a depth-first traversal of the octree structure. This ordering is equivalent to a Morton order of the boxes as described e.g. in [34], which, as indicated in that contribution, can be generated quickly from the positions $\mathbf{k} \in I_B^D$ of the level- D boxes $B_{\mathbf{k}}^D$ through a bit-interleaving procedure. Ordering the surface discretization points according to the Morton order of the containing level- D boxes also guarantees a Morton order on every other level d , $1 \leq d \leq D$. More precisely, at every level d the Morton order introduces a total order \prec on the set of boxes. The ordering of the surface discretization points Γ_N is facilitated by assigning each point $x \in \Gamma_N$ the Morton order of the containing level- D box, which can be computed through a division operation on the coordinates of the point x to get the index $\mathbf{k} \in I_B^D$ of the containing box with a subsequent bit-interleaving procedure, followed by a simple sorting of the points according to their assigned Morton order. Noting that the map which assigns to each point on Γ_N the Morton order of the containing level- D box is not injective, in order to obtain a total order on all of Γ_N we additionally order in an arbitrary manner subset of points $x \in \Gamma_N$ with the same assigned Morton order. The resulting overall order has the desirable properties that, on every level d , surface discretization points within any given box are contiguous in memory, and that boxes close in real space are also close in memory.

The sorted surface discretization points are distributed to the MPI ranks based on their containing level- D boxes, in such a way that the boxes processed by each each rank are an “interval” set of the form $\{B \in \mathcal{R}_B^D : B_{\mathbf{k}_1}^D \prec B \prec B_{\mathbf{k}_2}^D\}$, for suitable choices of $\mathbf{k}_1, \mathbf{k}_2 \in I_B^D$ designed to guarantee that all the boxes on a given rank contain a number of surface discretization points as close as possible to the average value N/N_r . Hence, the smallest boxes in the octree structure represent the smallest “unit” for the distribution of the surface discretization points. The maximum possible deviation in the number of discretization points assigned to a certain MPI rank from the average is therefore given by the maximum number of surface discretization points contained within one level- D box in the octree structure. For reasonable distributions of the discretization points Γ_N on the surface Γ , and for a suitable choice of the number of levels D , this deviation between MPI ranks is typically less than 100 surface discretization points.

The set of *surface discretization points stored in the ρ -th MPI rank*, $1 \leq \rho \leq N_r$, is denoted by $\Gamma_{N,\rho}$. By definition, the subsets $\Gamma_{N,\rho}$ of Γ_N are pairwise disjoint and their union over all MPI

Algorithm 9 MPI Parallel LevelDEvaluations

```
1: parallel for  $C_{\mathbf{k};\gamma}^D \in \mathcal{R}_{C,\rho}^D$  do  
2:   Evaluate and store  $F_{\mathbf{k}}^D(\mathcal{X}C_{\mathbf{k};\gamma}^D)$   
3:   Generate interpolant  $IPC_{\mathbf{k};\gamma}^D$   
4: end parallel for
```

Algorithm 10 MPI Parallel Interpolation(d)

```
1: parallel for  $x \in \Gamma_{N,\rho}$  do  
2:   for  $B_{\mathbf{k}}^d \in \mathcal{M}^d(x)$  do  
3:     Determine  $C_{\mathbf{k};\gamma}^d$  s.t.  $x \in C_{\mathbf{k};\gamma}^d$   
4:     Evaluate  $IPC_{\mathbf{k};\gamma}^d(x) \times G(x, x_{\mathbf{k}}^d)$   
5:   end for  
6: end parallel for
```

ranks $\rho = 1, \dots, N_r$ equals Γ_N . The distribution of the surface discretization points is used to evenly divide between all MPI ranks the work performed in the *Interpolation* function (OpenMP Algorithm 8). The underlying level- D based distribution of Γ_N is utilized throughout all levels $d = D, \dots, 3$. Thus, the MPI parallel *Interpolation* function results from the straightforward and level-independent modification of Line 1 in Algorithm 8, to read $x \in \Gamma_{N,\rho}$ instead of $x \in \Gamma_N$ —as shown in Algorithm 10. Naturally, the values of the discrete operator $I(x_\ell)$ in (1) computed by the ρ -th MPI rank correspond to points $x_\ell \in \Gamma_{N,\rho}$, and they are therefore also stored in the ρ -th MPI rank. In other words, the set of resulting field values $I(x_\ell)$ is partitioned and stored in the MPI ranks according to the partition utilized for the surface discretization points Γ_N .

The data associated with the level- d relevant cone segments is also distributed to MPI ranks on the basis of a total order—in this case, a total order on the set of level- d cone segments that is based on the Morton order imposed on the level- d boxes, in such a way that co-centered cone segments are close in memory. It should be noted that, for every relevant cone segment $C_{\mathbf{k};\gamma}^d \in R_C^d$, $3 \leq d \leq D$ (see (5)), the set of P coefficients that characterize the polynomial interpolants $IPC_{\mathbf{k};\gamma}^d$ (Section 2), which approximate the field $F_{\mathbf{k}}^d$ in (3) within the cone segment $C_{\mathbf{k};\gamma}^d$, need to be stored, in appropriately distributed manner, for two consecutive levels. Indeed, for each d , these level- d coefficients are utilized to enable two different interpolation procedures, namely interpolation from level d to interpolation points at the parent-level ($d - 1$) in the *Propagation* function (Line 4

Algorithm 11 MPI Parallel Propagation(d)

```
1: parallel for  $C_{\mathbf{j};\gamma}^{d-1} \in \mathcal{R}_{C,\rho}^{d-1}$  do  
2:   for  $B_{\mathbf{k}}^d \in \mathcal{C}(\mathcal{R}_B C_{\mathbf{j};\gamma}^{d-1})$  do  
3:     for  $x \in \mathcal{X}C_{\mathbf{j};\gamma}^{d-1}$  do  
4:       Determine  $C_{\mathbf{k};\alpha}^d$  s.t.  $x \in C_{\mathbf{k};\alpha}^d$   
5:       Evaluate and add  $IPC_{\mathbf{k};\alpha}^d(x) \times G(x, x_{\mathbf{k}}^d)/G(x, x_{\mathbf{j}}^{d-1})$   
6:     end for  
7:   end for  
8:   Generate interpolant  $IPC_{\mathbf{j};\gamma}^{d-1}$   
9: end parallel for
```

in Algorithm 7), as well as interpolation to the level- d cousin surface discretization points in the *Interpolation* function (Line 3 in Algorithm 8).

The set of level- d relevant cone segments \mathcal{R}_C^d is sorted on the basis of the Morton order induced by the co-centered (level- d) boxes followed by a suitable sorting in accordance with the position of the cone segments in the spherical coordinate system originating at the box center, resulting in a total order \sqsubset in the set of all level- d relevant cone segments. (The co-centered cones are ordered using the radial direction first, then elevation and finally azimuth, although any other ordering could be used among cone segments co-centered with a given box.) Finally, at each level d ($d = D, \dots, 3$), approximately equi-sized and pair-wise disjoint intervals of relevant cone segments C of the form $\{C \in \mathcal{R}_C^d : C_{\mathbf{k}_1; \gamma_1}^d \sqsubset C \sqsubset C_{\mathbf{k}_2; \gamma_2}^d\}$, for some $\mathbf{k}_1, \mathbf{k}_2 \in I_B^d$ and $\gamma_1, \gamma_2 \in I_C^d$ (i.e., disjoint intervals of *contiguous* cone segments) are distributed to the MPI ranks. As is the case for the relevant boxes, the proposed ordering of the relevant cone segments implies that cone segments which are close in real space (i.e. co-centered with the same box and pointing in the same direction or co-centered with boxes which are close in real space) are also close in memory, and, in particular, are likely to be stored within the same MPI rank. Analogously to the notation introduced above for the distributed surface discretization points, the relevant level- d cone segments assigned to a MPI rank with index ρ , $1 \leq \rho \leq N_r$, are denoted by $\mathcal{R}_{C, \rho}^d$. The MPI-capable algorithm is thus obtained by adjusting the loops in the first lines in Algorithms 6 and 7 to only iterate over the level- d relevant cone segments $\mathcal{R}_{C, \rho}^d$ stored in the current rank ρ , as shown in the MPI parallel Algorithms 9 and 11, instead of iterating over all relevant cone segments on level d .

3.2.2 Practical implementation of the box-cone data structures

A C++ implementation of the parallel IFGF box-cone data structures described above, which enables a linearithmic memory and time complexity, is described in detail in what follows.

In the proposed implementation the geometry Γ_N is stored in three separate arrays X_1 , X_2 and X_3 (either C style arrays or `std::vector`) of size N for the x_1 , x_2 , and x_3 components of the surface discretization points $(x_1, x_2, x_3) = x \in \Gamma_N$, resulting in a *structure of arrays* (SoA) memory layout [35], which is beneficial as it leads to increased floating-point performance under automatic vectorization on the basis of *single instruction, multiple data* (SIMD) hardware [27, Section 2.7] generally available in modern processors. As mentioned above in Section 3.2.1, each one of the three arrays is sorted according to the Morton order of the boxes. Similarly, the real and imaginary parts of the resulting field values $I(x_\ell)$, $1 \leq \ell \leq N$, are stored as two independent arrays, I_{\Re} and I_{\Im} , of size N . The order of these field values coincides with the order imposed on the surface discretization points such that $I(x_\ell) = I_{\Re}[k] + \iota I_{\Im}[k]$ at a given point x_ℓ is stored at the same position k in the arrays I_{\Re} and I_{\Im} as the corresponding surface discretization point $x_\ell = (X_1[k], X_2[k], X_3[k])$ in the arrays X_1 , X_2 and X_3 .

The algorithm enacts the box-octree inherent in the IFGF solver in the form of a *linear octree structure* (cf. [36, 37]). In particular, the proposed linear octree only includes data associated with relevant boxes, and it does not store any information about non-relevant boxes, to avoid $\mathcal{O}(N^{3/2})$ memory requirements, as described in detail in what follows. Relevant boxes in the linear octree are represented, on each level $d = 3, \dots, D$, by the box index $\mathbf{k} \in I_B^d$ (as described above in Section 2) and the equivalent Morton order. Each box stores the position in the arrays X_1 , X_2 , and X_3 of the first surface discretization point contained in the box in addition to the number of discretization points in the box in a hash map (cf. [36, Section 11]) with average $\mathcal{O}(1)$ time and memory complexity for read access (e.g. a `std::unordered_map`), where the Morton order of the box is utilized as the

key. Thus, given a Morton order of a box, the discretization points contained within the box can be determined in $\mathcal{O}(1)$ time and memory complexity. Conversely, given any surface discretization point $x \in \Gamma_N$, the three-dimensional index $\mathbf{k} \in I_B^d$ (for every level $d = 3, \dots, D$) of the box $B_{\mathbf{k}}^d$ containing the point x and the associated Morton order can be determined through simple division and bit-interleaving, as described in Section 3.2.1, in $\mathcal{O}(1)$ time and memory. Overall, this guarantees a true $\mathcal{O}(N \log N)$ time and memory implementation by avoiding the storage of any information regarding non-relevant boxes. Note that the linear octree structure described above is essentially the same as the one presented in [34].

Similarly, for each level d , the relevant cone segments $C_{\mathbf{k};\gamma}^d$, or, more precisely, the real and imaginary parts of the P coefficients representing the interpolants $I_P C_{\mathbf{k};\gamma}^d$ on the relevant cone segments $C_{\mathbf{k};\gamma}^d$, are stored separately in two one-dimensional arrays per rank (following the above partition of the cone segments to the ranks). To associate the three-dimensional cone segment index $\gamma \in I_C^d$ with the actual coefficients, a hash map for each relevant box $B_{\mathbf{k}}^d$ is used, where the *value* of the hash map is an index pointing to the first of the coefficients $I_P C_{\mathbf{k};\gamma}^d$ in the array of coefficients mentioned above, and where $\gamma \in I_C^d$ is the *key* of the hash map. (Note that the three-dimensional cone segment index γ , which runs over both relevant and non-relevant cone segments, corresponds to the relative position of the cone segment in the spherical coordinate system centered at the box center.) The usage of a hash map circumvents the storage of any non-relevant cone segment data while maintaining the association with the three-dimensional index γ that allows an easy identification of the cone segment based on its relative position in spherical coordinates. Thus, for a given Cartesian point $x \in \mathbb{R}^3$, this data structure can be used to locate the interpolant $I_P C_{\mathbf{k};\gamma}^d$ for the relevant cone segment $C_{\mathbf{k};\gamma}^d \in R_C^d$ containing the point x through a transformation of x to spherical coordinates centered at the origin of the cone segment $C_{\mathbf{k};\gamma}^d$, a division to get the cone segment index γ and a look-up in the hash map to get the coefficients of the interpolating polynomial. The association of any point with the relevant cone segment containing it can therefore be achieved on average in $\mathcal{O}(1)$ time and memory. This is required in the *Interpolation* and *Propagation* function to facilitate the interpolation to cousin surface discretization points and parent-level interpolation points, respectively.

Note that, for increased performance, the hash maps described above and stored on a given rank ρ are required to contain all associations between boxes, cone segments, discretization points and interpolation coefficients utilized by the current rank ρ at any point in the algorithm. In particular, if certain surface discretization points or interpolant coefficients are stored on a different rank $\tilde{\rho} \neq \rho$, but are required in the current rank ρ , the above hash maps are utilized to find the data and, consequently, enable the communication of that data through MPI. While this produces some data duplication, analogously to “halo regions” [27, Sec. 9.6] employed in grid-based methods, the memory duplicated in the parallel IFGF method is limited to surface discretization points and interpolant coefficients of neighbors and cousins.

3.2.3 Data communication

Clearly, for an MPI rank to access data stored in a different rank, explicit communication between the ranks must take place. The proposed solution, which we favor due to the decreased complexity of the implementation it entails, is based on *one-sided* or *remote memory access* (RMA) communication introduced in MPI-2 [26, Section 5], [27, Section 8]—which utilizes a single MPI.Get or MPI.Put call on the origin rank instead of a coupled MPI.Recv-MPI.Send call (or similar functionalities) involving both the origin and the target rank.

The data any MPI rank may require from other MPI ranks is limited to certain interpolants $I_{PC_{\mathbf{k};\gamma}^d}$. It is therefore sufficient to store the corresponding coefficients in so-called RMA *windows* (in MPI given by `MPI_Win` and allocated with e.g. `MPI_Win_allocate`), which enable the one-sided communication approach. For increased efficiency, the computations and communications are organized among the ranks on the basis of the following two considerations: 1) For each ρ , $1 \leq \rho \leq N_r$, the ρ -th rank asynchronously collects from other ranks all the data (i.e. the coefficients of the interpolants) it requires to perform *Interpolation* or *Propagation* computations assigned to it; and 2) The communications necessary to collect this data are interleaved with the computations in such a way that while the computations by the *Interpolation* function take place, the communication for the next *Propagation* function is performed and vice versa. This approach, which effectively hides the communications behind computations (thus increasing the performance and parallel efficiency), requires every MPI rank to store all data it obtains from other ranks for one full level- d ($3 \leq d \leq D$) *Interpolation* or *Propagation* step while it continues to store the coefficients it has itself generated—which effectively increases the peak memory per rank requirements slightly (by e.g. 10% or less).

The level- d dependent *CommunicateInterpolationData* (resp. *CommunicatePropagationData*) programming function in Algorithm 12 (resp. Algorithm 13) encapsulates the communications performed by each rank to obtain, from other ranks, the polynomial coefficients it needs to enact the necessary level- d interpolation computations (resp. interpolation computations onto level- $(d - 1)$ interpolation points) required by the *Interpolation* (resp. *Propagation*) function. The *LevelDEvaluations* function does not need any communications since the surface discretization points $x \in \Gamma_N$, which are required in the *LevelDEvaluations* function but which are not stored as part of $\Gamma_{N,\rho}$ (see previous Section 3.2.1), are duplicated to the ρ -th MPI rank. The rank that stores a level- D relevant cone segment, as described at the beginning of Section 3.2, facilitates the evaluation of the field at the interpolation points of that cone segment and the generation of the interpolants independently from every other MPI rank.

Using the functions 9 through 13, the pseudo-code for the proposed overall MPI-OpenMP IFGF algorithm is given in Algorithm 14. Note that access to RMA windows is usually asynchronous and requires some form of synchronization to ensure the data transfer is finalized before the communicated data is accessed. Moreover, the call to the *CommunicatePropagationData* in Algorithm 14 requires for the *Propagation* function to have completed in all ranks targeted by the communication function.

3.3 Parallel linearithmic complexity analysis

Reference [1, Sec. 3.3.3] shows that the basic IFGF algorithm runs on a linearithmic ($\mathcal{O}(N \log N)$) number of arithmetic operations. The present section, in turn, shows that the *communication cost* additionally required by the proposed MPI-OpenMP parallel IFGF algorithm also grows linearithmically—thus, establishing that, on a fixed number of cores, the parallel algorithm runs on an linearithmic overall computing time.

To do this, in view of the data distribution strategy described in Section 3.2.1, it suffices to ensure that both the *Interpolation* and *Propagation* functions require a linearithmic communication cost. Inspection of the corresponding Algorithms 10 and 11 (specifically, lines 4 and 5, respectively) shows that these functions, and, thus, the overall parallel IFGF algorithm, only require communication of certain polynomial coefficients—a task that is effected via the communication Algorithms 13 and 12, respectively. Thus, the analysis of the communication cost amounts to counting the number of coefficients that are communicated, including multiple counts for coefficients that are communicated

to multiple ranks, as a result of the application of these two communication algorithms within the overall IFGF algorithm.

In order to count the number of communications effected by each one of these algorithms we proceed as follows. Noting that, since, 1) As indicated in [1, Sec. 3.3.3], there are $\mathcal{O}(N)$ relevant cone segments per level, each one of which contains $\mathcal{O}(1)$ data (namely, the P coefficients of a single polynomial interpolant); 2) Each cone-segment data is stored in exactly one MPI rank (Section 3.2.1); and, as discussed below for both communication algorithms, 3) Each relevant cone segment is communicated to a uniformly bounded number of MPI ranks at each level $d = 3, \dots, D$; it follows that for each level d ($3 \leq d \leq D$) a total of $\mathcal{O}(N)$ coefficients are communicated by each of the communication algorithms 12 and 13 for each one of the $D = \log N$ levels, at a total communication cost of $\mathcal{O}(N \log N)$ coefficients by this algorithm, as desired.

It remains for us to show that point 3) above holds for both communication algorithms. In the case of the propagation communication we note that each relevant cone segment on any level $d = D, \dots, 4$ is split into eight smaller cone segments on the parent level ($d - 1$). Thus, for each level- d relevant cone segment, this results in at most K parent-level cone segments (usually $K = 8$, or possibly a slightly higher number owing to the re-centering procedure associated with the *Propagation* function, but most often $K = 1$) that could be targets for the interpolation procedure in the *Propagation* function. In view of point 2) above, each level- d relevant cone segment must thus communicate coefficients to no more than $\mathcal{O}(1)$ ranks, and point 3) follows in this case.

In the case of the interpolation communication, finally, relevant cone-segment coefficients need to be communicated to ranks that store surface discretization points included in boxes that are cousins of the box co-centered with the relevant cone segment. First, on the lowest level D , each relevant box has at most $K = 189$ cousin boxes and since, by design, the surface discretization points contained within each one of the smallest boxes are stored in a single MPI rank (Section 3.2.1), it follows that $\mathcal{O}(1)$ (at most 189) different MPI ranks require coefficients contained in each relevant cone segment. Further, since each cone segment is partitioned into eight in the transition from a given level d to a subsequent level ($d - 1$) (so that the number of relevant level- D boxes contained within a level- $(d - 1)$ cone equals approximately one-fourth of the corresponding number for level- d cone segments, since Γ_N is a discretization of a 2D surface), and since, conversely, the number of MPI ranks storing surface discretization points within a cousin box increases by approximately a factor four in the same d -to- $(d - 1)$ transition, the number of communications per relevant cone segment remains essentially constant as a result of the d -to- $(d - 1)$ level transition. It follows that each relevant cone segment is communicated to a $\mathcal{O}(1)$ number of MPI ranks for all levels d , thus establishing the validity of point 3) for the interpolation communication function, and completing the proof of linearithmic complexity of the proposed parallel IFGF algorithm.

4 Numerical Results

Our numerical examples focus on three simple geometries which coincide with the test cases presented in [1]: a sphere of radius a , the oblate spheroid $x^2 + y^2 + (z/0.1)^2 = a^2$ and the prolate spheroid $x^2 + y^2 + (z/10)^2 = a^2$. The latter two geometries are depicted in Figure 2. In what follows the diameter (also referred to as the “size”) of a geometry Γ is denoted by

$$d := d(\Gamma) := \max_{x, y \in \Gamma} |x - y|, \quad (9)$$

Algorithm 12 CommunicatePropagationData(d)

```
1: parallel for  $C_{\mathbf{j};\gamma}^{d-1} \in \mathcal{R}_{C,\rho}^{d-1}$  do
2:   for  $B_{\mathbf{k}}^d \in \mathcal{C}(\mathcal{R}_B C_{\mathbf{j};\gamma}^{d-1})$  do
3:     for  $x \in \mathcal{X} C_{\mathbf{j};\gamma}^{d-1}$  do
4:       Find  $\tilde{\gamma}$  such that  $x \in C_{\mathbf{k};\tilde{\gamma}}^d \in \mathcal{R}_C B_{\mathbf{k}}^d$ 
5:       Identify the MPI rank  $\rho$  on which  $I_P C_{\mathbf{k};\tilde{\gamma}}^d$  is stored
6:       MPI_Get  $I_P C_{\mathbf{k};\tilde{\gamma}}^d$  from rank  $\rho$ 
7:     end for
8:   end for
9: end parallel for
```

Algorithm 13 CommunicateInterpolationData(d)

```
1: parallel for  $x \in \Gamma_{N,\rho}$  do
2:   for  $B_{\mathbf{k}}^d \in \mathcal{M}^d(x)$  do
3:     Find  $\tilde{\gamma}$  such that  $x \in C_{\mathbf{k};\tilde{\gamma}}^d \in \mathcal{R}_C B_{\mathbf{k}}^d$ 
4:     Identify the MPI rank  $\rho$  on which  $I_P C_{\mathbf{k};\tilde{\gamma}}^d$  is stored
5:     MPI_Get  $I_P C_{\mathbf{k};\tilde{\gamma}}^d$  from rank  $\rho$ 
6:   end for
7: end parallel for
```

(not to be confused with the level index d introduced in Section 2); clearly we have $d = 2a$ in the case of the sphere and the oblate spheroid geometries and $d = 20a$ for the prolate spheroid geometry. These relatively simple geometries present the same kinds of challenges, in the context of the IFGF method, that arise in a wide range of real-world problems, including aircraft, lenses and meta-materials (with a point distribution somewhat similar to that in an oblate spheroid), submarines (prolate spheroid), etc. For example, even though the problem of finding a scattering solution for a submarine is much more challenging than the corresponding problem for a spheroid of the same size, in view of the need for accurate integration of singular kernels and adequate representation of the surface Jacobians, the performance of the IFGF method for the evaluation of the discrete

Algorithm 14 IFGF Method

```
1: LevelDEvaluations()
2: CommunicatePropagationData( $D$ )
3:
4: for  $d = D, \dots, 3$  do
5:   CommunicateInterpolationData( $d$ )
6:   if  $d > 3$  then
7:     Propagation( $d$ )
8:     if  $d > 4$  then
9:       CommunicatePropagationData( $d - 1$ )
10:    end if
11:   end if
12:   Interpolation( $d$ )
13: end for
```

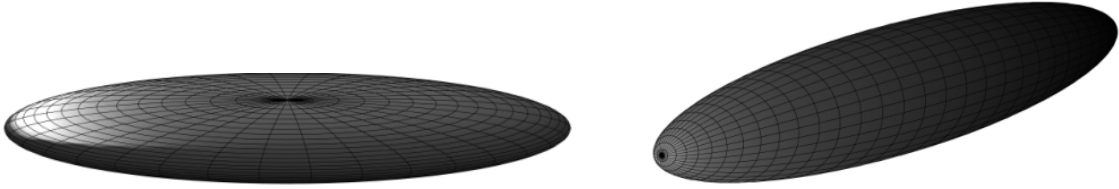


Figure 2: Test geometries. Left: Oblate spheroid $x^2 + y^2 + (z/0.1)^2 = a^2$. Right: Prolate spheroid $x^2 + y^2 + (z/10)^2 = a^2$.

operator (1) for a submarine should not differ significantly from the corresponding performance on a prolate spheroid of a comparable discretization, point distribution and electromagnetic size.

In what follows we present IFGF performance data based on various runs for these geometries. For our examples we utilize discretizations Γ_N obtained from use of parametrized surface patches covering Γ and equispaced partitioning of the corresponding parameter spaces. The computer used is described briefly prior to the beginning of Section 3.1 and, in more detail, in the Supplementary Materials Section SM1.1. The strong and weak efficiency and speedup scalability concepts are detailed in Section SM1.4; briefly, relative to a base core-number N_c^0 , the N_c -core run speedup $S_{N_c^0, N_c}$ and the weak and strong efficiencies $E_{N_c^0, N_c}^w$ and $E_{N_c^0, N_c}^s$ are used to characterize the effectiveness of the proposed parallelization schemes by relating computing times and core numbers under weak-scaling tests (in which N_c is increased proportionally to the size N of the discretization Γ_N) and strong-scaling tests (wherein N_c is increased as N is held fixed).

Γ	N	d	Nodes	N_c	ε	T (s)	E_{56, N_c}^w (%)	$E_{\frac{N_c}{4}, N_c}^w$
Sphere	1, 572, 864	128λ	1	56	2×10^{-3}	7.77×10^1	100	-
	6, 291, 456	256λ	4	224	2×10^{-3}	9.78×10^1	87	87
	25, 165, 824	512λ	16	896	2×10^{-3}	1.34×10^2	69	79
Oblate Spheroid	1, 572, 864	128λ	1	56	7×10^{-4}	2.99×10^1	100	-
	6, 291, 456	256λ	4	224	6×10^{-4}	4.17×10^1	79	79
	25, 165, 824	512λ	16	896	8×10^{-4}	5.74×10^1	62	79
Prolate Spheroid	6, 291, 456	256λ	1	56	5×10^{-4}	4.97×10^1	100	-
	25, 165, 824	512λ	4	224	6×10^{-4}	6.83×10^1	79	79
	100, 663, 296	$1,024\lambda$	16	896	7×10^{-4}	9.29×10^1	63	79

Table 1: Weak scaling test transitioning from 1 to 4 nodes, and then from 4 to 16 nodes, for three different geometries. The number of nodes, each one containing $N_c = 56$ cores, is kept proportional to the number of surface discretization points, as required by the weak-scaling paradigm.

Table 1 demonstrates the weak IFGF parallel efficiency, for all three geometries considered, from a single compute node ($N_c^0 = 56$) to 4 and 16 compute nodes ($N_c = 224$ and 896 , respectively). We find that the efficiency relative to the base $N_c^0 = 56$ case steadily decreases, but, importantly, the weak relative efficiency $E_{\frac{N_c}{4}, N_c}^w$ remains essentially constant as N_c increases. Thus, under the assumption that this trend is maintained for arbitrarily large numbers of nodes (as is expected in view of the discussion in the first paragraph of Section 3.2 concerning absence of hard limitations on achievable parallelism), the parallel IFGF method is applicable to arbitrarily large problems—

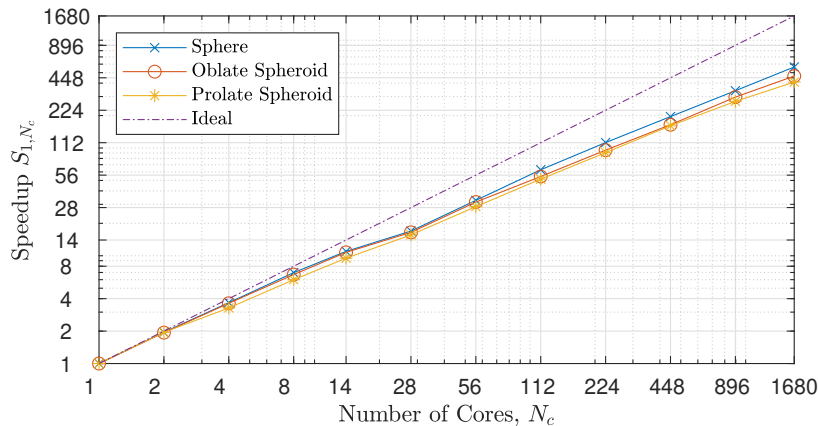


Figure 3: Measured speedup S_{1,N_c} (vertical axis) versus number of cores N_c (horizontal axis) in a strong scaling test transitioning from 1 core to 1,680 cores (= 30 compute nodes) for three geometries: a sphere of size 128 wavelengths (blue), an oblate spheroid of size 128 wavelengths (red), and prolate spheroid of size 256 wavelengths (yellow). The dash-dotted purple line indicates the theoretical perfect speedup.

provided correspondingly large hardware is used—with a constant $\approx 80\%$ efficiency factor (cf. Table 1) as the problem and hardware sizes are both quadrupled from a given point of reference. Section SM1.5 demonstrates a similar quality of the proposed algorithm under strong-scaling tests.

The observed speedups under strong scaling tests, in turn, are displayed in Figure 3; additional details concerning these results are provided in Section SM1.5. This figure presents speedup tests for three test cases: a sphere of diameter $d = 128\lambda$ (where $\lambda = \frac{2\pi}{\kappa}$ denotes the wavelength and d is given in (9)), and oblate and prolate spheroids (Figure 2) of large diameters $d = 128\lambda$ and $d = 256\lambda$, respectively. The curves in Figure 3 display, in each case, the observed speedup S_{1,N_c} for $1 \leq N_c \leq 1,680$. In view of the requirements of the strong-scaling setup, test problems were selected that can be run in a reasonable time on a single core and with the memory available in the corresponding compute node. Clearly, such test problems tend to be too small to admit a perfect distribution onto large numbers of cores. As illustrated in Figure 3, however, in spite of this constraint, excellent scaling is observed in the complete range going from 1 core to 1,680 cores (30 nodes). As in the weak-scaling tests, further, there is no hard limitation on scaling, even for such small problems, (once again, in line with the discussion presented in Section 3), and it is reasonable to expect that, unlike other approaches (for which either hard limits arise [14] as described in the first paragraph of Section 3.3, or which rely on memory duplication [16, 17]), and we expect the observed speedup continues to scale with the number of cores, as suggested by Figure 3, up to very large numbers of cores. The computing speedups achieved by the proposed parallel strategy outperform those achieved by other MPI-parallel implementations of FMM and other numerical methods [18, 20, 38], and can be best appreciated by noting that, instead of the e.g. approximately 40 minutes (2.54×10^3 secs., see first line in Table SM1 in Section SM1.5) required by a single-core IFGF run, a total of 4.5 secs. ($4.5 = 2.54 \times 10^3 / S_{1,1680}$ secs., where, per Figure 3, $S_{1,1680} = 565$) suffices for the corresponding 1,680-core IFGF run. It is interesting to note that an approximately 1.51 second 1,680-core run would have resulted under perfect scaling.

Concluding this section, Figure 4 presents results of an investigation regarding the linearithmic scaling of the parallel IFGF method for the prolate spheroid geometry on a fixed number of nodes, namely, all 30 nodes available in the computer cluster we use, and for N ranging from 6,291,456

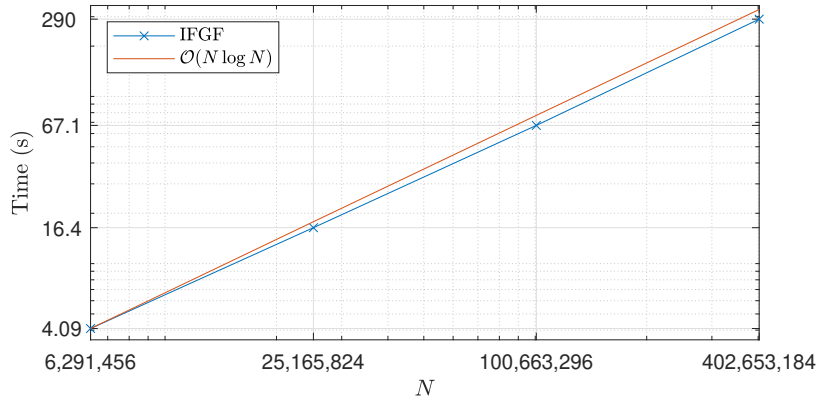


Figure 4: Illustration of the linearithmic complexity of the parallel IFGF method (which had previously been demonstrated [1] for the serial version of the algorithm), for the prolate spheroid geometry, on 30 compute nodes, with error $\varepsilon \approx 1.5 \times 10^{-2}$. The acoustic diameter of the ellipsoid is kept proportional to \sqrt{N} , and it ranges from 512λ to $4,096\lambda$. Clearly, the parallel implementation preserves (and, in fact, slightly improves upon) the ideal linearithmic scaling. For this test one MPI rank per node and 56 OpenMP threads per MPI rank were used (resulting in 1680 cores). The peak IFGF memory used per MPI rank (excluding the memory required to store the initial geometry) as well as other additional data in tabular form are presented in Table SM4.

to 402,653,184, for corresponding diameters ranging from 512λ to $4,096\lambda$. The data in this figure, which is also presented in tabular form in Table SM4, was generated by pinning a single MPI rank to each compute node, each of which spawns 56 OpenMP threads, with parameters resulting in an IFGF error $\varepsilon \approx 1.5 \times 10^{-2}$ (cf. equation (SM2)). The results show that the linearithmic algorithmic complexity and memory requirements of the basic IFGF algorithm are maintained in the parallel setting. Indeed, the observed complexity even slightly outperforms the postulated $\mathcal{O}(N \log N)$ within this range of values of N ; cf. Table SM4 which suggests convergence to exact linearithmic complexity as N grows.

5 Concluding Remarks

This paper presented a parallel version of the IFGF acceleration method introduced in [1], demonstrating in practice excellent parallel scaling to large core numbers while simultaneously preserving the linearithmic complexity of the sequential IFGF algorithm. The proposed parallelization approach exploits the box-cone octree structure inherent in the IFGF method, resulting in a strategy that, per the theoretical discussion in Section 3.1 and in the first paragraph of Section 3.2, is applicable to arbitrarily large number of processing cores, and it thereby does not suffer from bottlenecks or hard limits inherent in approaches that orchestrate the parallelization on the basis of octree-box partitioning only. A number of additional questions are left for future work, as briefly mentioned in what follows. On one hand, the feasibility of implementations on heterogeneous architectures such as, e.g., computer systems that incorporate general purpose graphical processing units (GPUs), is currently under study. In particular, the use of GPUs to accelerate the interpolation processes, which represent the most time consuming part of the IFGF method, appears as highly promising avenue of inquiry. Additionally, minor modifications to the data-decomposition strategy introduced in Section 3.2.1 could be introduced to not only (approximately) equipartition the surface discretiza-

tion points among MPI ranks, but also equipartition the number of actual computations and the amount of data required from other MPI ranks. Such an improved data-decomposition design could indeed be obtained by relying on minor adjustments to the cone and box intervals introduced in Section 3.2.1 leading to improved load-balancing, and, thus, improved parallel efficiency.

Acknowledgments

This work was supported by NSF, DARPA and AFOSR through contracts DMS-2109831 and HR00111720035 and FA9550-21-1-0373, and by the NSSEFF Vannevar Bush Fellowship under contract number N00014-16-1-2808.

References

- [1] Christoph Bauinger and Oscar Bruno. “Interpolated Factored Green Function” method for accelerated solution of scattering problems. *Journal of Computational Physics*, 430, 01 2021.
- [2] Björn Engquist and Lexing Ying. Fast directional multilevel algorithms for oscillatory kernels. *Journal of Scientific Computing*, 29(4):1710–1737, 2007.
- [3] Emmanuel J. Candès, Laurent Demanet, and Lexing Ying. A fast butterfly algorithm for the computation of fourier integral operators. *Multiscale Model. Simul.*, 7:1727–1750, 2009.
- [4] Eric Michielssen and Amir Boag. A multilevel matrix decomposition algorithm for analyzing scattering from large structures. *IEEE Transactions on Antennas and Propagation*, 44(8):1086–1093, 1996.
- [5] V. Rokhlin. Diagonal forms of translation operators for the helmholtz equation in three dimensions. *Applied and Computational Harmonic Analysis*, 1(1):82 – 93, 1993.
- [6] Hongwei Cheng, William Y. Crutchfield, Zydrunas Gimbutas, Leslie F. Greengard, J. Frank Ethridge, Jingfang Huang, Vladimir Rokhlin, Norman Yarvin, and Junsheng Zhao. A wideband fast multipole method for the helmholtz equation in three dimensions. *Journal of Computational Physics*, 216:300–325, 2006.
- [7] Steffen Börm and Jens Melenk. Approximation of the high-frequency helmholtz kernel by nested directional interpolation. *Numerische Mathematik*, 137(1):1–37, 10 2017.
- [8] Steffen Börm. Directional h2-matrix compression for high-frequency problems. *Numerical Linear Algebra with Applications*, 24, 07 2017.
- [9] Oscar P. Bruno and Leonid A. Kunyansky. A fast, high-order algorithm for the solution of surface scattering problems: Basic implementation, tests, and applications. *Journal of Computational Physics*, 169:80–110, 2001.
- [10] E. Bleszynski, M. Bleszynski, and T. Jaroszewicz. Aim: Adaptive integral method for solving large-scale electromagnetic scattering and radiation problems. *Radio Science*, 31(5):1225–1251, 1996.

- [11] Joel R. Phillips and Jacob K. White. A precorrected-fft method for electrostatic analysis of complicated 3-d structures. *IEEE Transactions on computer-aided design of integrated circuits and systems*, 16(10):1059–1072, 1997.
- [12] Lexing Ying, George Biros, Denis Zorin, and M. Harper Langston. A new parallel kernel-independent fast multipole method. In *A New Parallel Kernel-Independent Fast Multipole Method*, 11 2003.
- [13] Mario Bebendorf and Sergej Rjasanow. Adaptive low-rank approximation of collocation matrices. *Computing*, 70:1–24, 02 2003.
- [14] Austin R. Benson, Jack Poulson, Kenneth Tran, Björn Engquist, and Lexing Ying. A parallel directional fast multipole method. *Journal of Scientific Computing*, 36(4):C335–C352, 2014.
- [15] A. Chandramowlishwaran, S. Williams, L. Oliner, I. Lashuk, G. Biros, and R. Vuduc. Optimizing and tuning the fast multipole method for state-of-the-art multicore architectures. In *2010 IEEE International Symposium on Parallel Distributed Processing (IPDPS)*, pages 1–12, 2010.
- [16] Rui-Qing Liu, Xiao-Wei Huang, Yu-Lin Du, Ming-Lin Yang, and Xin-Qing Sheng. Massively parallel discontinuous galerkin surface integral equation method for solving large-scale electromagnetic scattering problems. *IEEE Transactions on Antennas and Propagation*, 69(9):6122–6127, 2021.
- [17] Ming-Lin Yang, Yu-Lin Du, and Xin-Qing Sheng. Solving electromagnetic scattering problems with over 10 billion unknowns with the parallel mlfa. In *2019 Photonics Electromagnetics Research Symposium - Fall (PIERS - Fall)*, pages 355–360, 2019.
- [18] Özgür Ergül and Levent Gurel. A hierarchical partitioning strategy for an efficient parallelization of the multilevel fast multipole algorithm. *IEEE Transactions on Antennas and Propagation*, 57(6):1740–1750, 2009.
- [19] Caleb Waltz, Kubilay Sertel, Michael A. Carr, Brian C. Usner, and John L. Volakis. Massively parallel fast multipole method solutions of large electromagnetic scattering problems. *IEEE Transactions on Antennas and Propagation*, 55(6):1810–1816, 2007.
- [20] Luis Landesa, Jose Taboada, Fernando Obelleiro, Jose Rodriguez, José Carlos Gallego, and Andres Gomez. Solution of very large integral-equation problems with single-level fmm. *Microwave and Optical Technology Letters*, 51:2451 – 2453, 10 2009.
- [21] Fangzhou Wei and Ali E. Yilmaz. A more scalable and efficient parallelization of the adaptive integral method—part i: Algorithm. *IEEE Transactions on Antennas and Propagation*, 62(2):714–726, 2014.
- [22] Fangzhou Wei and Ali E. Yilmaz. A more scalable and efficient parallelization of the adaptive integral method—part ii: Bioem application. *IEEE Transactions on Antennas and Propagation*, 62(2):727–738, 2014.

- [23] Miloš Nikolić, Aleksandar Jović, Josip Jakić, Vladimir Slavnić, and Antun Balaž. *An Analysis of FFTW and FFTE Performance*, pages 163–170. Springer International Publishing, Cham, 2014.
- [24] Nail A. Gumerov and Ramani Duraiswami. *Fast Multipole Methods for the Helmholtz Equation in Three Dimensions*. Elsevier Science, 2004.
- [25] Jack Poulson, Laurent Demanet, Nicholas Maxwell, and Lexing Ying. A parallel butterfly algorithm. *Journal of Scientific Computing*, 36(1):C49–C65, 2014.
- [26] Thomas Rauber and Gudula Rünger. *Parallel Programming*. Springer, Berlin, Heidelberg, 2 edition, 2013.
- [27] T. Sterling, M. Brodowicz, and M. Anderson. *High Performance Computing: Modern Systems and Practices*. Elsevier Science, 2017.
- [28] Mark Bull, James Enright, Xu Guo, Chris Maynard, and Fiona Reid. Performance evaluation of mixed-mode OpenMP/MPI implementations. *International Journal of Parallel Programming*, 38:396–417, 10 2010.
- [29] N. Drosinos and N. Koziris. Performance comparison of pure mpi vs hybrid mpi-openmp parallelization models on smp clusters. In *18th International Parallel and Distributed Processing Symposium, 2004. Proceedings.*, pages 15–, 2004.
- [30] Dana Akhmetova, Roman Iakymchuk, Orjan Ekeberg, and Erwin Laure. Performance study of multithreaded mpi and openmp tasking in a large scientific code. In *2017 IEEE International Parallel and Distributed Processing Symposium Workshops (IPDPSW)*, pages 756–765, 2017.
- [31] F.M. Dekking, C. Kraaikamp, H.P. Lopuhaä, and L.E. Meester. *A Modern Introduction to Probability and Statistics: Understanding Why and How*. Springer Texts in Statistics. Springer, 2005.
- [32] James Reinders, Ben Ashbaugh, James Brodman, Michael Kinsner, John Pennycook, and Xinmin Tian. *Data Parallel C++: Mastering DPC++ for Programming of Heterogeneous Systems using C++ and SYCL*. Springer Nature, 2021.
- [33] P.S. Pacheco. *An Introduction to Parallel Programming*. Morgan Kaufmann, 2011.
- [34] M.S. Warren and J.K. Salmon. A parallel hashed oct-tree n-body algorithm. In *Supercomputing '93: Proceedings of the 1993 ACM/IEEE Conference on Supercomputing*, pages 12–21, 1993.
- [35] Amanda K Sharp. Memory layout transformations. <https://www.intel.com/content/www/us/en/developer/articles/technical/memory-layout-transformations.html>. Accessed: 2021-12-20.
- [36] T.H. Cormen, C.E. Leiserson, R.L. Rivest, and C. Stein. *Introduction to Algorithms*. MIT Press, 2009.
- [37] Hanan Samet. *The Design and Analysis of Spatial Data Structures*. Addison-Wesley Longman Publishing Co., Inc., USA, 1990.

- [38] Miguel Ruiz-Cabello N., Maksims Abalēnkovs, Luis M. Diaz Angulo, Clemente Cobos Sanchez, Franco Moglie, and Salvador G. Garcia. Performance of parallel fdtd method for shared- and distributed-memory architectures: Application to bioelectromagnetics. *PLOS ONE*, 15(9):1–16, 09 2020.

Supplementary materials for “Massively Parallelized Interpolated Factored Green Function Method”

Christoph Bauinger* and Oscar P. Bruno*

SM1 Supplementary Numerical Results

The present supplementary numerical results section expands on Section 4 in various ways. In particular, this section provides details on the hardware employed and the manner in which it is used (Sections SM1.1 and SM1.2, respectively), and, after detailing the method used for error evaluation (Section SM1.3) and the concepts used to evaluate strong and weak parallel efficiency (Section SM1.4), it presents detailed strong parallel scaling results in Section SM1.5 and data regarding the linearithmic ($\mathcal{O}(N \log N)$) scaling tests in Section SM1.6.

SM1.1 Compiler and hardware

The proposed parallel IFGF program was implemented in C++, and the resulting code was compiled with the Intel mpiicpc compiler, version 2021.1, and the Intel MPI library. The following performance-relevant compiler flags were used: `-std=c++20`, `-O3`, `-ffast-math`, `-qopt-zmm-usage=high`, `-no-prec-sqrt`, `-no-prec-div`. All tests were run on our internal *Wavefield* cluster which consists of 30 dual-socket nodes. Each node consists of two Intel Xeon Platinum 8276 processors with 28 cores per processor, i.e. 56 cores per node, and 384 GB of GDDR4 RAM per node. (The Xeon processors we use support hyper-threading, but this capability was not exploited in any of our tests presented in this paper.) The nodes are connected with HDR Infiniband.

SM1.2 Hardware pinning

As indicated in Section 3, since each compute node in the *Wavefield* cluster consists of four NUMA nodes, we run four MPI ranks per node each pinned to one of these four NUMA nodes through setting the environment variable `“I_MPI_PIN_DOMAIN=cache3”`. The shared memory parallelization with OpenMP is then used for the parallelization within each MPI rank, i.e., within a NUMA node. The parallel scaling within a NUMA node from 1 to 14 cores is investigated below using the OpenMP specific environment variables `“OMP_NUM_THREADS=[1-14]”`, `“OMP_PLACES=cores”`, and `“OMP_PROC_BIND=true”`. The continued scaling, which is achieved with the MPI parallelization when exceeding 14 cores, is investigated going from one to four MPI ranks (each rank pinned to one NUMA node in the same compute node), which corresponds to the MPI scaling on a single, shared-memory node. Finally, the scaling of the MPI based distributed-memory parallelization is

*Computing and Mathematical Sciences, Caltech, Pasadena, CA 91125, USA

investigated starting from a single node to 16 nodes, where each node is fully utilized with four MPI ranks per node and fourteen cores per rank, as described above. A different hardware pinning used for the test cases presented in Section SM1.6 is described separately in that section.

SM1.3 Numerical error estimation

The errors reported in what follows were computed as indicated in [1], that is, the relative L_2 difference ε_M between the full, non-accelerated evaluation of the field $I(x)$, as stated in (1), and the IFGF-accelerated evaluation $I_{\text{acc}}(x)$ of (1) is computed on a randomly chosen subset of M surface discretization points. More precisely, the error is given by

$$\varepsilon_M = \sqrt{\frac{\sum_{i=1}^M |I(x_{\sigma(i)}) - I_{\text{acc}}(x_{\sigma(i)})|^2}{\sum_{i=1}^M |I(x_{\sigma(i)})|^2}}, \quad (\text{SM1})$$

where σ is a random permutation and $x_\ell \in \Gamma_N$ denote the surface discretization points. The method used in [1] is suitably extended to the present MPI parallel implementation by using a set of test points x_ℓ that contains a number $M = 1000$ of randomly chosen points on each MPI rank. (In [1] it was shown for sufficiently small examples that an error evaluation on a subset of 1000 points produces an error estimation close to the actual error.) More precisely, 1000 surface discretization points are randomly chosen on each MPI rank from the distinct set of surface discretization points $\Gamma_{N,\rho}$ each MPI rank ρ ($1 \leq \rho \leq N_r$) is responsible for based on the distribution introduced in Section 3.2. The final errors are then accumulated resulting in the overall error estimate

$$\varepsilon := \varepsilon_M \quad \text{at } M = 1000 \times N_r \text{ points.} \quad (\text{SM2})$$

As a result, the errors are dependent on the number N_r of MPI ranks, which is the reason the shown errors vary slightly as the number of MPI ranks varies (cf. Tables SM2 and SM3). All tests were set up in such a way that an error of approximately 10^{-3} is achieved, although, the IFGF method can achieve arbitrarily small errors.

SM1.4 Weak and strong parallel efficiency concepts

Let $T(N_c, N)$ denote the time required by a run of the parallel IFGF algorithm on an N -point discretization Γ_N , with a given and fixed discretization scheme, of a given surface Γ using N_c cores. Using this notation, for a given N , the strong parallel efficiency $E_{N_c^0, N_c}^s$ that results as the number of cores is increased from N_c^0 to N_c is defined as the quotient of the resulting speedup $S_{N_c^0, N_c}$ to the corresponding ideal speedup value $S_{N_c^0, N_c}^{\text{ideal}}$:

$$S_{N_c^0, N_c}^{\text{ideal}} := \frac{N_c}{N_c^0}, \quad S_{N_c^0, N_c} := \frac{T(N_c^0, \Gamma_N)}{T(N_c, \Gamma_N)}, \quad E_{N_c^0, N_c}^s := \frac{S_{N_c^0, N_c}}{S_{N_c^0, N_c}^{\text{ideal}}}.$$

Note that the implicit dependence on N and Γ_N is suppressed in the speedup and efficiency notations.

Γ	N	d	N_c	ε	T (s)	E_{1,N_c}^s (%)	S_{1,N_c}
Sphere	1, 572, 864	128λ	1	2×10^{-3}	2.54×10^3	100	1.00
			2		1.29×10^3	98	1.95
			4		6.91×10^2	92	3.67
			8		3.63×10^2	87	6.98
			14		2.31×10^2	78	10.98
Oblate Spheroid	1, 572, 864	128λ	1	5×10^{-4}	9.42×10^2	100	1.00
			2		4.86×10^2	97	1.94
			4		2.60×10^2	91	3.62
			8		1.40×10^2	84	6.69
			14		8.76×10^1	77	10.75
Prolate Spheroid	6, 291, 456	256λ	1	6×10^{-4}	1.42×10^3	100	1.00
			2		7.29×10^2	97	1.95
			4		4.33×10^2	82	3.28
			8		2.37×10^2	75	5.99
			14		1.49×10^2	68	9.49

Table SM1: Strong parallel scaling test of the OpenMP IFGF implementation from $N_c = 1$ to $N_c = 14$ cores in a single node for three different geometries Γ .

The weak parallel efficiency $E_{N_c^0, N_c}^w > 0$, in turn, concerns the computing costs that are observed as the numbers N_c of cores are increased proportionally to the problem size N —effectively keeping the number of surface discretization points per core constant—so that as the numbers of cores and discretization points are simultaneously increased from N_c^0 to N_c and from N^0 to N , respectively, the relation

$$N/N^0 = N_c/N_c^0 \quad (\text{SM3})$$

is satisfied. Since the weak scaling concerns varying numbers N of surface discretization points, however, the weak parallel-efficiency concept must correctly account for the linearithmic theoretical scaling of the IFGF algorithm. To do this, we consider the computing time $T(N_c, N)$ required for a run of the algorithm on N_c cores for an N -point discretization of a given, fixed, surface Γ . In view of the linearithmic complexity of the algorithm, perfect weak parallel efficiency would be observed if, for a certain constant K , we had

$$T(N_c, N) = \frac{K}{N_c} N \log N.$$

Thus is to say, under perfect weak parallel scaling, in view of (SM3) we would have

$$\frac{T(N_c, N)}{T(N_c^0, N^0)} = \frac{N_c^0 N \log N}{N_c N^0 \log N^0} = \frac{\log N}{\log N^0},$$

We therefore define the *weak parallel efficiency* that results as the number of cores is increased from N_c^0 to N_c by

$$E_{N_c^0, N_c}^w := \frac{T(N_c^0, N^0) \log N}{T(N_c, N) \log N^0}.$$

Note that $E_{N_c^0, N_c}^w = 1$ corresponds to perfect weak parallel efficiency, or a weak parallel efficiency of 100%.

Γ	N	d	N_r	N_c	ε	T (s)	E_{14, N_c}^s (%)	S_{14, N_c}
Sphere	1, 572, 864	128λ	1	14	2×10^{-3}	2.31×10^2	100	1.00
			2	28	2×10^{-3}	1.49×10^2	77	1.54
			4	56	2×10^{-3}	7.77×10^1	74	2.97
Oblate Spheroid	1, 572, 864	128λ	1	14	5×10^{-4}	8.76×10^1	100	1.00
			2	28	6×10^{-4}	5.71×10^1	77	1.53
			4	56	6×10^{-4}	2.99×10^1	73	2.93
Prolate Spheroid	6, 291, 456	256λ	1	14	6×10^{-4}	1.49×10^2	100	1.00
			2	28	6×10^{-4}	9.10×10^1	82	1.65
			4	56	5×10^{-4}	4.97×10^1	75	3.01

Table SM2: Strong parallel scaling test of the shared-memory MPI implementation on a single node, transitioning from $N_c = 14$ cores to $N_c = 56$ (all cores available in one compute node) by increasing the number N_r of MPI ranks from 1 to 4, for three different geometries Γ .

SM1.5 Strong parallel efficiency tests

Tables SM1, SM2, and SM3 present the strong parallel efficiencies achieved by the proposed parallel IFGF method under OpenMP, shared-memory MPI, and distributed-memory MPI parallelization strategies, respectively, each one for all three test geometries considered in this section. In detail, these tables display the main two strong parallel performance quantifiers, namely the observed strong parallel efficiency $E_{N_c^0, N_c}^s$ and speedup $S_{N_c^0, N_c}$, along with the computing times T , the obtained accuracy ε , and details concerning the geometry and the discretizations. The tables clearly show that, in all cases, the IFGF parallel efficiencies are essentially independent of the geometry type. With reference to Section SM1.2 above, the ranges of the parameter N_c considered in these tables span all of the available cores in each one of the relevant hardware units used: 14 cores in a single NUMA node, 56 cores (4 NUMA nodes) in a single compute node, and 16 nodes in the complete cluster (the largest number of nodes which equals a power of 2 in the cluster used).

The largest efficiency deficit observed as a result of a hardware-doubling transition is the decrease by a full 23% (from 100% to 77%) shown in Table SM2, which results from the transition from one to two MPI ranks (that is, from one to two 14-core NUMA nodes). We argue that this deficit, which takes place precisely as an MPI communication between NUMA nodes is first introduced, is not a sole reflection of the character of the algorithm in presence of the MPI interface, since such large deficits are not observed in any other MPI related hardware-doubling transitions reported in the various tables. As potential additional contributing elements to this deficit we mention notably, MPI overhead (which would only be incurred in the first doubling transition but not in subsequent doubling transitions, in view of the decreasing number of pairwise communications incurred by the algorithm under a doubling transition in a strong scaling test, as indicated by the theoretical discussion in Section 3.3), and the Intel Turbo Boost Technology inherent in the processors used—which achieve maximum turbo frequencies when running under lower loads, and which, when concurrently using larger numbers of cores in a single node, cease to operate.

Γ	N	d	N_c	ε	T (s)	E_{56, N_c}^s (%)	S_{56, N_c}	$E_{\frac{N_c}{2}, N_c}^s$
Sphere	6, 291, 456	256λ	56	2×10^{-3}	3.55×10^2	100	1.00	-
			112	2×10^{-3}	1.80×10^2	99	1.97	99
			224	2×10^{-3}	9.78×10^1	91	3.64	92
			448	2×10^{-3}	5.52×10^1	81	6.44	89
			896	2×10^{-3}	3.12×10^1	71	11.40	89
Oblate Spheroid	6, 291, 456	256λ	56	6×10^{-4}	1.34×10^2	100	1.00	-
			112	6×10^{-4}	7.41×10^1	91	1.81	91
			224	6×10^{-4}	4.17×10^1	80	3.22	89
			448	6×10^{-4}	2.38×10^1	70	5.64	88
			896	6×10^{-4}	1.40×10^1	60	9.56	85
Prolate Spheroid	25, 165, 824	512λ	56	4×10^{-4}	2.23×10^2	100	1.00	-
			112	5×10^{-4}	1.22×10^2	92	1.83	92
			224	6×10^{-4}	6.83×10^1	82	3.28	89
			448	6×10^{-4}	3.74×10^1	75	5.97	91
			896	6×10^{-4}	2.23×10^1	63	10.01	84

Table SM3: Strong parallel scaling test of the distributed-memory MPI implementation from $N_c = 56$ to $N_c = 896$ cores (1 to 16 compute nodes) with 4 MPI ranks per node for three different geometries Γ .

A variety of other data is presented in these tables. Tables SM1 and SM2, which demonstrate the strong scaling within a single NUMA node, and among all four NUMA nodes within a compute node, are included for completeness, but as discussed below, we attach far greater significance to Table SM3, which demonstrates the scaling of the method under the one hardware element that can truly be increased without bounds, namely, the number of compute nodes. In this table, geometries twice as large than those used for the previous two tables are considered (to reasonably increase the minimum computing times), and the hardware is scaled from one compute node to sixteen compute nodes. Per the description in Section SM1.2, each node is assigned four MPI ranks, each one of which is pinned to one of the four NUMA nodes present in the compute node. Overall, a strong scaling efficiency of over 60% can be observed in all cases, with the results of the sphere test case even above 70% owing to the symmetry of the geometry and the resulting increased load-balance and minimized communication between ranks. The loss of efficiency can be attributed the load-imbalance induced by our data partitioning strategy, the communication between ranks, and the parallelization overhead introduced by MPI and OpenMP.

The most important quality illustrated in these tables is the IFGF’s efficiency performance under strong-scaling hardware-doubling transitions demonstrated in the last column of Table SM3. This performance, which mirrors the corresponding weak-scaling performance presented in the last column of Table 1, shows that, as in the weak scaling case, under the assumption that the displayed trend is maintained for large numbers of nodes (below the obvious limit imposed by the fixed problem size), the parallel IFGF method for a fixed problem can be efficiently run in large numbers of computing cores—with an efficiency factor no worse than a constant $\approx 80\%$ as the hardware sizes are doubled from a given point of reference.

The character of the IFGF algorithm under weak- and strong-scaling hardware-doubling tests,

as discussed above in this section and in Section 3.3, would ensure that, provided the demonstrated trends are maintained (as is expected in view of the discussion in the first paragraph of Section 3.2), the method can be executed successfully in very large hardware infrastructures.

SM1.6 Linearithmic scaling

Table SM4, finally, presents numerical data related to the test case considered in Figure 4, which concerns the linearithmic scaling of the parallel IFGF method on a fixed and large number of cores. As indicated in Section 4, the data in the figure and table were generated by pinning a single MPI rank to each compute node, each of which spawns 56 OpenMP threads on each one of the 30 nodes available in the computer cluster we use, with parameters resulting in an IFGF error $\varepsilon \approx 1.5 \times 10^{-2}$ (cf. equation (SM2)). The observed complexity slightly outperforms the postulated $\mathcal{O}(N \log N)$ estimate within this range of values of N . Note, in particular, the last column of Table SM4 which suggests rapid convergence to exact linearithmic complexity, with a well defined proportionality constant, as N grows.

Γ	N	d	N_c	ε	T (s)	Mem/rank	$T/(N \log N)$
Prolate Spheroid	6,291,456	512λ	1,680	1.5×10^{-2}	4.09×10^0	0.50 GB	9.56×10^{-8}
	25,165,824	$1,024\lambda$			1.64×10^1	1.89 GB	8.83×10^{-8}
	100,663,296	$2,048\lambda$			6.71×10^1	7.42 GB	8.33×10^{-8}
	402,653,184	$4,096\lambda$			2.90×10^2	29.73 GB	8.37×10^{-8}

Table SM4: Preservation of the linearithmic IFGF scaling in the parallel context. One MPI rank per node and 56 OpenMP threads per MPI rank on 30 compute nodes for a prolate spheroid geometry were used for this test. The peak memory per MPI rank used by the IFGF method (excluding the memory required to store the initial geometry) is listed in the next-to-last column. The value in the last column suggests convergence to exact $\mathcal{O}(N \log N)$ scaling.

References

- [1] C. Bauinger and O. Bruno. “Interpolated Factored Green Function” method for accelerated solution of scattering problems. *Journal of Computational Physics*, 430, 01 2021.